AGU ADVANCING EARTH AND SPACE SCIENCES

Earth and Space Science

RESEARCH ARTICLE
10.1029/2025EA004207

Lightning Density and Its Coupled Covariates Within the Continental United States

Steffen Eisenacher[1], Anke Fluhrer[1,2], Jan Bliefernicht[1], Daniel J. Short Gianotti[3], Harald Kunstmann[1,4], and Thomas Jagdhuber[1,2]

[1]Institute of Geography, University of Augsburg, Augsburg, Germany, [2]German Aerospace Center (DLR), Microwaves and Radar Institute, Weßling, Germany, [3]Department of Civil and Environmental Engineering, Massachusetts Institute of Technology (MIT), Cambridge, MA, USA, [4]Institute for Meteorology and Climate Research, Karlsruhe Institute of Technology, Garmisch-Partenkirchen, Germany

Key Points:

- CAPE is the most effective proxy for lightning density across the U.S., especially in the summer
- Soil moisture is strongly coupled with lightning in the southeastern U.S., and more weakly in arid southwestern regions
- Soil moisture variations show a significant lagged seasonal effect on lightning density, especially during summer months

Correspondence to:

A. Fluhrer and T. Jagdhuber,
anke.fluhrer@dlr.de;
thomas.jagdhuber@dlr.de

Citation:

Eisenacher, S., Fluhrer, A., Bliefernicht, J., Short Gianotti, D. J., Kunstmann, H., & Jagdhuber, T. (2025). Lightning density and its coupled covariates within the Continental United States. *Earth and Space Science*, *12*, e2025EA004207. https://doi.org/10.1029/2025EA004207

Received 13 JAN 2025
Accepted 24 JUN 2025

Author Contributions:

Conceptualization: Thomas Jagdhuber
Data curation: Steffen Eisenacher, Anke Fluhrer
Formal analysis: Steffen Eisenacher, Anke Fluhrer, Daniel J. Short Gianotti, Thomas Jagdhuber
Funding acquisition: Jan Bliefernicht, Harald Kunstmann
Investigation: Steffen Eisenacher
Methodology: Steffen Eisenacher, Thomas Jagdhuber
Project administration: Harald Kunstmann
Supervision: Anke Fluhrer, Jan Bliefernicht, Daniel J. Short Gianotti, Thomas Jagdhuber
Visualization: Steffen Eisenacher, Anke Fluhrer
Writing – original draft: Steffen Eisenacher

Abstract Lightning is a critical climate variable, due to both its significance as a metric of atmospheric thresholding and its significance as a natural hazard. While lightning density is often studied as a marker of local convective dynamics, it is also a player in the larger coupled systems linking the local atmospheric column, the land surface, and dynamic moisture advection. Aiming to bridge the land-atmosphere gap in lightning studies, the research investigates the interplay between soil moisture (SM), convective available potential energy (CAPE), precipitation, wind shear, atmospheric moisture, and lighting density. Employing spatial correlations (r) and year-over-year change analyses, satellite (SMAP) and reanalysis (ERA5 and NARR) data from 2016 to 2021 show the seasonal and interannual co-evolution of lightning and its land-atmosphere covariates. Across the continental United States (CONUS), CAPE was identified as the most effective proxy for lightning density, particularly in summer ($r = 0.80$). Notably, the southeastern U.S. displayed a significant connection between SM and lightning ($r = 0.60$), representing the role of thunderstorms in seasonal land surface moisture as well as feedbacks from the land surface to convective processes upstream of lightning. In contrast, the arid southwestern U.S., another region of high thunderstorm occurrence, exhibited reduced correlations with SM ($r = 0.12$), likely due to both the reduced persistence of moisture anomalies in arid regions and the relatively weaker land surface feedbacks compared to the influence of advection by the North American monsoon. The coupling of SM was most pronounced in the southeastern U.S. during the summer months (JJA), while no clear pattern was identifiable elsewhere within CONUS. Wavelet analyses suggest seasonal changes in the lead-lag behavior of SM and lightning density, with SM commonly leading in the Southeast in JJA. Year-to-year change analysis during JJA revealed aligning trends, reinforcing the relationship between summertime SM and lightning. This study provides a baseline reference for coupled land and atmosphere feedbacks between terrestrial lightning, its precursors, and its effects.

1. Introduction

Lightning is one of Earth's most intense natural phenomena. The electrical discharges that occur during thunderstorms cause thousands of deaths each year and substantial damage to infrastructure (GCOS, 2023). Lightning is not only a valuable indicator for tracking and understanding trends in climate variability and change based on thunderstorm activity, but it also has a direct link to convection (Brisson et al., 2021; R. Zhang et al., 2017). Due to its ability to produce nitrogen oxides, lightning has a direct impact on the global climate (Aich et al., 2018; GCOS, 2023; Price, 2013). Consequently, lightning was introduced by The Global Climate Observing System as a new essential climate variable in 2018 (Aich et al., 2018). Thunderstorms typically require three primary ingredients, with a fourth ingredient determining their severity. The main three are moisture, instability, and lifting (Doswell et al., 1996; McNulty, 1985; NOAA, 2023), while vertical wind shear enables thunderstorms to organize and become more severe (Kaltenböck et al., 2009; Williams, 2017).

Williams (2017) states that terrestrial moisture sources like water bodies and soils are crucial for thunderstorm development as they add necessary moisture to the atmosphere. Atmospheric instability, quantified as positive CAPE, plays a key role in thunderstorm initiation and is closely connected to the available water and heat in the atmosphere, due to the effects of latent heat release and turbulent surface heating of the atmospheric boundary layer (Doswell et al., 1996; Emanuel, 2023; McNulty, 1985; Williams, 2017). Instability in the lower atmosphere, represented by positive CAPE, promotes upward air motion, deep convection, and the development of thunderstorms (Westermayer et al., 2017; Williams, 2017).

Writing – review & editing: Anke Fluhrer, Jan Bliefernicht, Daniel J. Short Gianotti, Harald Kunstmann, Thomas Jagdhuber

The initiation of thunderstorms requires upward motion, triggered by various mechanisms (Doswell et al., 1996; NOAA, 2023; Williams, 2017). Fronts, such as cold fronts, warm fronts, dry lines, and outflow boundaries, create lift by separating air masses with differences in density. Differential heating, exemplified by phenomena like sea breeze convergence, also contributes to thunderstorm development by generating lift along boundaries between turbulent flux regimes, such as water to land, soil moisture gradients, and land cover transitions. Other triggering mechanisms include orographic lifting and moisture advection (Doswell et al., 1996; NOAA, 2023).

Vertical wind shear (VWS), the fourth factor influencing thunderstorm severity, involves an increase in wind speeds with altitude. VWS causes thunderstorms to tilt, separating updrafts and downdrafts, with high VWS extending a storm's duration. Thunderstorms in low VWS conditions are brief and termed "air mass" or "pop-up storms," while those in high VWS environments are more severe, potentially producing hail and organizing into mesoscale convective systems. Strong directional shear can lead to supercells, characterized by rotating mesocyclones, capable of persisting for up to 12 hr (Kaltenböck et al., 2009; Williams, 2017). Past research on lightning and its covariates has primarily centered around CAPE, highlighting its significant role in determining convection triggering and influencing lightning density (Dewan et al., 2017; Westermayer et al., 2017). Romps et al. (2018) found that the product of CAPE and precipitation is a reliable proxy for estimating lightning activity, both at the regional level in the contiguous United States (CONUS) and globally over land. However, this relationship does not hold over the ocean. Tippett et al. (2019) confirmed the utility of the product of CAPE and precipitation but noted that it performs better on shorter time scales, such as daily or monthly periods, and is less effective during the warm season when lightning is more common. CAPE is broadly considered to be upstream of convection events and generally causal, as convection tends to use and dissipate CAPE.

While previous studies have predominantly used CAPE as the dominant continental lightning covariate, the field of land-atmosphere coupling demonstrates that there are many other complex interactions between convection cycle and the water and energy cycles at the land-air interface (Betts, 2009; Guo et al., 2006; Lintner et al., 2013; J. Zhang et al., 2008). One crucial variable is SM, playing a pivotal role in the lower atmosphere's moisture content and influencing instability and CAPE (Klein & Taylor, 2020; L. Zhang et al., 2023). Soil moisture contributes to total column water vapor (TWV) through latent heat fluxes, which then feeds back on CAPE generation, atmospheric stability, and the land surface energy balance.

This study aims to bridge the land-atmosphere gap by focusing on these variables in relation to CAPE and examining how the coupled land-atmosphere states drive and respond to lightning density. Hereby, the study focuses on CAPE, SM, TWV, and VWS, as these variables physically govern key aspects of convective storm development, including instability, moisture supply, and storm organization (all abbreviations can be found again in Table A1). The analyses will be conducted at monthly and seasonal temporal resolutions within CONUS using spatial correlations to understand linear relationships, and exploratory methods such as masked correlations and scatterplots to qualitatively assess potential non-linear dependence structures between variables from 2016 to 2021. More specifically, CONUS provides an ideal setting to compare regional variations in the relationship between lightning and these variables. Lastly, the study intends to assess the effects of year-over-year changes among these variables.

2. Data Base and Study Area

The study is performed for the contiguous United States using multiple atmospheric data sets (Table 1). In the following a description of the selected atmospheric data sets, the analyzed variables and study domain is given.

2.1. Data Sets and Variables

The lightning information is taken from the World Wide Lightning Location Network (WWLLN), which is a global lightning detection system designed to provide real-time lightning strike data across the world (Kaplan & Lau, 2021). It was initiated by the University of Washington in 2004 and currently consists of around 70 lightning detection stations, with a concentration in the Continental United States (CONUS). Ground-based remote sensing of lightning, such as WWLLN, primarily relies on the microwave range (3–30 kHz) for lightning detection, with very low frequency (VLF) and low frequency (LF) signals being key for cloud to ground strokes. WWLLN uses the "time-of-arrival" principle, which requires lightning stroke detection by at least five surrounding sensors for efficient geolocation. The National Lightning Detection Network (NLDN), a competitor on a national level, has a higher detection efficiency for both cloud-to-ground and inter/intra-cloud strokes, but imposes critical limitations

Table 1
List of Selected Data Sets Together With Their Original Spatial and Temporal Resolution, Period of Availability, and Type (LD = Lightning Density, SM = Soil Moisture, VWS = Vertical Wind Shear, CAPE = Convective Available Potential Energy, TWV = Total Column Water Vapor, P = Precipitation, SPEI = Standardized Precipitation Evaporation Index, NLCD = National Land Cover Database)

Data sets	Variable(s)	Type	Spatial resolution	Temporal resolution	Period	Reference
WWLLN/WGLC	LD	Ground- based	0.5°	Daily	2010–2021	Kaplan and Lau (2021)
SPL3SMP	SM	Satellite	36 km	Daily	03/2015-present	O'Neill et al. (2021a)
NARR	VWS	Reanalysis	0.25°	6-hourly	1980-present	Mesinger et al. (2006)
ERA5	CAPE, TWV, P	Reanalysis	0.25°	6-hourly	1940-present	Hersbach et al. (2020)
SPEI	SPEI	Model	0.5°	1-month	1901- present	SPEI (2023)
NLCD	Land cover	Satellite	30 m	3 years	2001- present	Dewitz and USGS (2021)

on data requests for research (Kaplan & Lau, 2021). The WWLLN facilitates spatial pattern analysis of lightning events globally, although it detects only a subset of all lightning strokes. Compared to regional networks, detection efficiency of WWLLN is lower but relatively consistent for spatial climatology purposes. For example, the WGLC captures about 15% of the lightning density observed by the Alaska Lightning Detection Network (Kaplan & Lau, 2021) and about 40% of the lightning density measured by the NLDN during peak lightning seasons over the continental United States (Kaplan & Lau, 2021). However, WGLC often detects greater lightning density than NLDN during the off-peak months, suggesting complementary detection characteristics. Importantly, the WGLC primarily detects high-energy strokes, whereas lower-energy strokes are more likely to be missed, as shown by median stroke power comparisons (Kaplan & Lau, 2021). Although regional differences exist, the relative spatial and seasonal patterns of lightning are preserved across data sets, and no consistent spatial bias was observed year-to-year. Therefore, while uncertainties in absolute lightning counts are acknowledged, WGLC remains appropriate for analyzing large-scale spatial and seasonal variability in lightning density, which is the focus of this study (Kang et al., 2022; Kaplan & Lau, 2021; Mezuman et al., 2014). For this study, WWLLN was chosen over NLDN due to its accessibility for research purposes. WWLLN data was preprocessed to create gridded lightning density maps for analysis. The data set is available at different temporal resolutions and covers the period from 2010 to 2021 and is denoted as the WWLLN Global Lightning Climatology (WGLC, Kaplan & Lau, 2021). The Soil Moisture Active Passive (SMAP) satellite, launched in January 2015, operates in a near-polar and sun-synchronous orbit at an altitude of 685 km. Equipped with a radiometer and (now inoperative) radar, the mission aims to retrieve global soil moisture data. The radiometer captures Earth's natural emission at L-band, allowing for precise measurements of soil moisture with a spatial resolution of 36 km (O'Neill et al., 2021b). SMAP's advanced acquisition system provides a revisit time of 2–3 days globally (O'Neill et al., 2021b). The SMAP Level 3 Radiometer Soil Moisture Version 8 data set (SPL3SMP) used in this study offers daily temporal resolution for CONUS and a spatial resolution of 36 km (Entekhabi et al., 2014). Utilizing the L-band for soil moisture estimation, SMAP's radiometer penetrates through vegetation effectively and measures microwaves originating from the upper portion of the soil column (Feldman et al., 2023). This study uses Level-3 data calculated by the Dual Channel Algorithm, which has accuracy improvements over older versions, particularly in agricultural areas (O'Neill et al., 2021b).

The analysis relies on the CAPE and total column water vapor (TWV) from ERA5 reanalysis data sets (Hersbach et al., 2023). ERA5, a global reanalysis data set from the European Center for Medium-Range Weather Forecasts (ECMWF), has a spatial resolution of 0.25° and temporal resolutions ranging from hourly to monthly since 1950. It integrates various observational sources, including weather stations, satellites, and balloons, utilizing the IFS (Integrated Forecast System) numerical model and data assimilation to adjust initial conditions for consistency with observational data (Hersbach et al., 2020). Since VWS is not directly provided by ERA5, this variable was sourced from the North American Regional Reanalysis (NARR) (Mesinger et al., 2006). NARR, gridded at 0.25° and available at 3-hr, daily, and monthly intervals, differs from ERA5 by employing the NCEP Eta Model with 45 layers. Similar to ERA5, NARR combines model outputs with the National Centers for Environmental Prediction (NCEP) Regional Data Assimilation System (RDAS) to produce accurate reanalysis data sets (Mesinger et al., 2006). There are trade-offs in using atmospheric variables from different reanalysis products. CAPE and TWV are expected to exhibit lower covariance with VWS because they originate from different underlying models, potentially reducing the signal-to-noise ratio in analyses. However, using independent reanalysis ensures

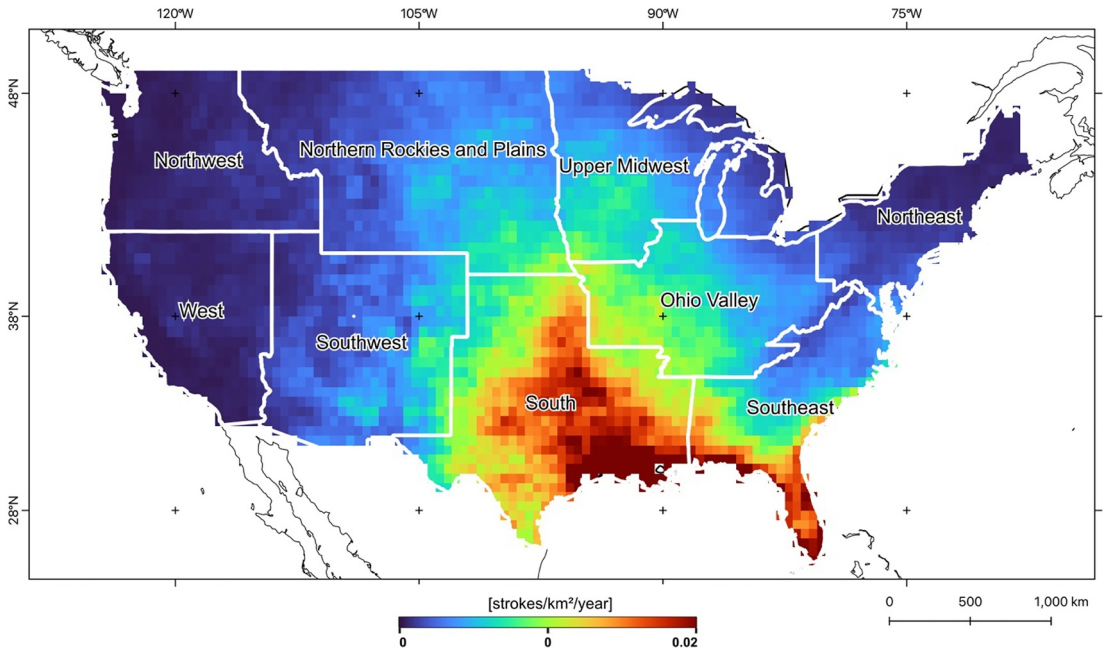

Figure 1. Contiguous United States climate regions after Koss and Karl (1984). Colors show lightning climatology from 2016 to 2021.

that any observed relationships between VWS and either CAPE or TWV are likely rooted in actual observations rather than shared model structures. Although this methodological choice enhances robustness against common modeling biases, it introduces risks of inconsistent dynamics among atmospheric variables, especially where those variables are closely coupled through model physics. Given computational limitations and restricted data access, this study could not perform a comprehensive subdomain sensitivity analysis comparing CAPE and VWS derived from ERA5 and NARR. Future research utilizing harmonized reanalysis products could more precisely attribute observed atmospheric patterns.

Furthermore, to interpret drought and precipitation patterns within CONUS, the Standardized Precipitation-Evapotranspiration Index (SPEI) product was obtained (SPEI, 2023). This product, derived from monthly precipitation and potential evapotranspiration data, provides information on drought conditions across timescales ranging from 1 to 48 months.

Additionally, land cover data from the National Land Cover Database (NLCD), a source offering landcover data across the CONUS at a 30 m resolution with 16 classes, was acquired (Dewitz and USGS, 2021).

2.2. Study Area

The study focuses on CONUS due to its diverse climate zones offering a platform to examine land-atmosphere interactions through the lens of lightning density. It also features a variety of thunderstorm lifting mechanisms (Doswell et al., 1996; NOAA, 2023), beneficial for investigations of how soil and atmospheric conditions and dynamics influence lightning. As identified by the National Centers for Environmental Information (NCEI) through comprehensive climate analysis (Koss & Karl, 1984), CONUS can be divided into nine distinct climate regions (Figure 1). While being used by the NCEI for climate anomaly analysis, the climate regions have also found use in many recent studies (Kunkel et al., 2020; Molina & Allen, 2020; Tippett et al., 2019). Due to their relative climatic consistency, these regions provide valuable opportunities to subdivide CONUS into separate regions for a more detailed examination of the studied variables and lightning density. Additionally, CONUS-based analyses benefit from extensive open data resources, including reliable reanalysis data and high-quality lightning detection networks as described in Section 2.1.

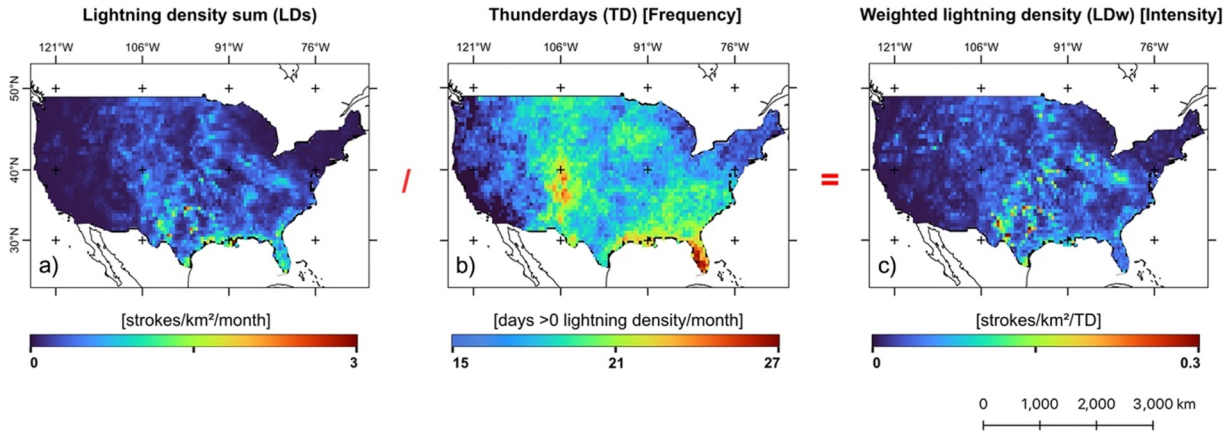

Figure 2. A comparison between the (total) lightning density LDs (a), (frequency) thunderdays TD (b), and weighted lightning density LD_w (c) in July 2016 over CONUS. The red symbols serve to illustrate the calculation of Equation 1.

3. Methods

The study was conducted from March 2015 (start of SMAP mission) to December 2021, aligning with the current end of the WGLC data set and runs at monthly temporal resolution serving as a baseline for temporal analyses. WGLC provides data at 0.5° spatial resolution. This is adopted as the standard for reprojecting the other data sets.

ERA5 data was obtained at 2 a.m., 8 a.m., 2 p.m., and 8 p.m., averaged for each day, and further aggregated to monthly averages. Similarly, WGLC and NARR daily data were aggregated to match these periods.

The study considered 360 days for each year, concluding on December 25th or 26th, depending on leap years. The calculation of monthly averages for all variables, including the WGLC, CAPE, TWV, SM, and VWS, was straightforward by using all available days of each month, except December where only 25 or 26 days were used.

Seasonal averages were computed for the different target variables of the study defining seasons as March, April, and May (MAM) for spring; June, July, and August (JJA) for summer; September, October, and November (SON) for autumn; and December, January, and February (DJF) for winter.

3.1. Thunderdays and Lightning Density

Throughout the analyses, we refer to "lightning density" (LD) as the number of lightning strokes per area per time. We decompose LD to calculate an additional variable, "thunderdays" (TD), quantifying the frequency of thunderstorms for each grid cell. TD is reported at the pixel scale in days with detected lightning per time window. Pixels with LD greater than zero were marked as valid thunderdays, while those equal to zero indicated no storms in that region for the day. This classification was applied to all raster cells of the daily grids and then aggregated to generate monthly patterns illustrating the number of days with thunderstorms per month. The results, depicted in Figure 2b for July 2016, underscored a significant distinction between LD (total lightning) and TD (frequency), emphasizing TD as an additional variable for exploring the relationship between coupled lightning interactions.

To additionally define an "intensity" metric, LD was normalized by thunderdays to compute the "weighted lightning density" LD_w:

$$LD_w = \sum_{i=1}^{n} \frac{LD_i}{TD_i}, \quad (1)$$

where n represents the total number of grid cells within the raster, i the specific grid cell. LD_w is thus the mean lightning density for only those days with thunderstorms.

In contrast, LD represents the daily average (strokes/km^2/day) calculated over the entire month or season using all available days.

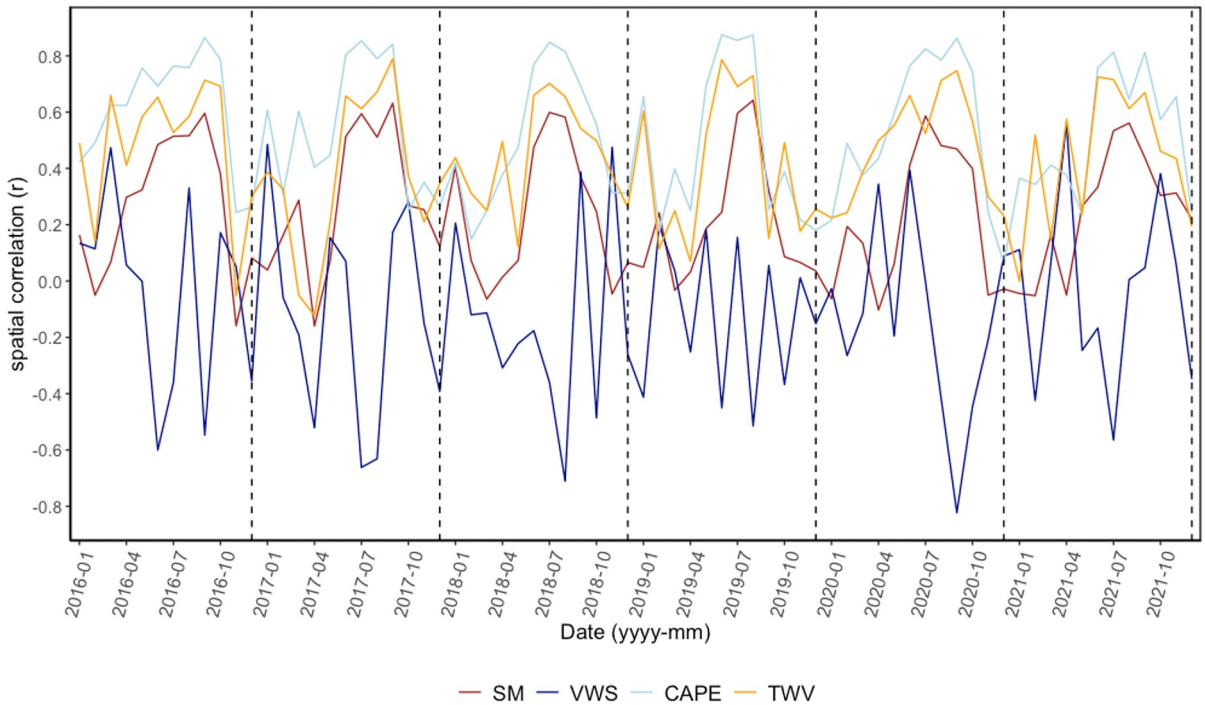

Figure 3. Spatial correlations between LD and each of SM, VWS, CAPE, and TWV for the Southeast climate region (Figure 1) based on monthly averages.

Figure 2c illustrates the weighted lightning density, LD_w. It is evident that the normalization of LD_w significantly reduces the values around the Florida peninsula, the Gulf of Mexico coast, and the regions east of the Rocky Mountains. Conversely, regions in the Midwest are enhanced in accordance with high LD and low TD. Areas with more thunderstorms will have higher TD. Those with more intense storms will have higher LD_w. Each of the three lightning variables (LD, TD, LD_w) may have different relationships and feedbacks with other coupled state variables.

3.2. Statistical Methods

In this research, a variety of statistical methods were utilized to examine the dependence structure between variables. Spatial correlations were computed as the primary method to assess spatial relationships between the variables, with the widely used Pearson correlation coefficient (r). Monthly or seasonal time series of each variable were utilized for analysis. For all pixels within a region, monthly or seasonal time-series of correlation coefficients were computed. For example, $r\left(\mathrm{LD}_{\substack{2018-07\\ \text{Southeast}}}, \mathrm{SM}_{\substack{2018-07\\ \text{Southeast}}}\right)$ is the spatial correlation across all pixels in the Southeast region between monthly LD and SM for July 2018. High values indicate strongly linear relationships between LD (e.g., Figure 2a) and monthly-averaged SM across pixels for that month. The time-series of monthly correlation coefficients for that region and pair of variables shows the variability of the relationship in time (Figure 3). To explore potentially non-linear interactions, correlations were also calculated using only the most extreme values of some variables (LD, TD, and SM these correlations are calculated only when a selected variable is above its 90th percentile). Masking by the upper decile of that is, TD, highlights locations with the most frequent thunderstorms on a monthly and seasonal basis. Time series and scatterplots were employed to visualize the results, and non-linear regression analysis was applied for a more detailed exploration of nonlinear patterns.

A year-over-year change Δx (for monthly and seasonal averages) was calculated to study changes in LD_w, LD, TD, and SM. Δx is retrieved by:

$$\Delta x = x_t - x_{t-1}, \tag{2}$$

where x_t is the value of the current year and x_{t-1} is the value for the previous year for the chosen variable.

Further analyses of ΔLD, ΔLD_w, and ΔTD were conducted by creating masks of ΔSM with positive and negative ΔSM, providing a detailed examination of how changes in lightning density and thunderstorm occurrence are related to interannual variations in soil moisture. Wavelet Coherence Analysis (WCA) was conducted to examine the dependency between lightning activity and soil moisture over a shorter temporal scale. WCA helps in studying lightning and soil moisture by revealing how their relationship changes over time and across different frequencies (Rahmati et al., 2020; Si, 2008). By identifying the time lags, specifically 1–15 days, WCA can show whether lightning activity changes typically precede soil moisture or follow it. This insight is crucial for understanding the dynamic interaction between soil moisture and lightning in greater detail.

4. Results

In the upcoming sections, the results will be presented and discussed. This includes a comprehensive analysis of the relationship between LD (and LD_w), SM, and instability related variables within the CONUS climate regions (Section 3.1.). In Section 3.2. Year-over-year changes of SM will be compared to the changes of LD and LD_w.

4.1. The Relationships Between Soil Moisture and Lightning Density Within CONUS

Thorough examinations were carried out across all climate regions (Figure 1), indicating that CAPE consistently displayed the strongest spatial correlations with lightning density in each region, closely trailed by TWV. The peak correlation coefficient between CAPE and LD averaged around $r = 0.8$ in each region, with the highest relationship being observed in the Southeast region, nearing $r = 0.9$ specifically during the summer months (Figure 3). This is interpreted spatially—those pixels with the highest lightning density also had the highest concurrent CAPE. TWV also shows a similarly strong relationship, with a notable peak correlation of 0.78 between LD and TWV in the Southeast.

Significant seasonal variability was observed for r(CAPE, LD) and r(TWV, LD) across both the study period and regions spanning from 2016 to 2021. This variability is depicted in Figure 3 for Southeast CONUS. Seasonal patterns strongly impact this variability, with a notable surge in thunderstorm activity during summer. LD declines in winter, due to lower winter temperatures, humidity, TWV, and CAPE, all of which diminish the potential for convective thunderstorms (Chen et al., 2020).

The Southeast region displays a strong correlation between LD and SM, while a noteworthy relationship with SM was not found in any other climate regions under investigation. In the JJA period, the association with SM ranges from $r = 0.5$ to 0.6. There are two reinforcing relationships at play here. (a) Most directly, thunderstorms are more common in the summer months, and so a larger fraction of SM variability is due to thunderstorm precipitation in those months, hence larger spatial correlations. (b) In the opposite causal direction, soil moisture is a source of water for the atmosphere, and is the primary control on sensible/latent heat partitioning over land (Short Gianotti et al., 2019), though oceans and lakes contribute significantly as well (Williams, 2017). This leads to build up of CAPE as water and heat are transferred from the soil to the lower atmosphere (L. Zhang et al., 2023), reinforcing convective activity. It is methodologically noteworthy that simple multivariate correlation analyses cannot distill the direct effect of SM on LD (or any coupled variables) without careful controls for exogenous variables and auto-correlation (Salvucci et al., 2002; Tuttle & Salvucci, 2017).

CAPE and SM demonstrate a higher correlation ($r = 0.79$) than SM-LD, highlighting the intermediary role the atmosphere plays in land-interactions with lightning. This could be due to (a) a more continuous, linear relationship between SM and CAPE, relative to the zero-inflated lightning data; (b) a physical role of SM upstream of lightning which is stronger than the proxy relationship between SM and LD via convective precipitation; or (c) a closer time-scale alignment between the auto-regressive (red-noise) soil moisture and CAPE processes on daily time-scales versus the thresholded LD process (Salvucci et al., 2002; L. Zhang et al., 2023).

The CAPE-LD (occurrence) correlations are generally stronger than the CAPE-LD_w (lightning intensity) correlations—by around 20% in the peak summer months, and more moving into the shoulder seasons. This is expected from both causal pathways above. Lightning occurrence is a strong proxy for convective precipitation and subsequent soil wetting. Additionally, previous studies tie instability and convective initiation—and hence lightning occurrence frequency (LD)—to CAPE and surface-layer variables, and tie storm intensity (LD_w) to

10.1029/2025EA004207

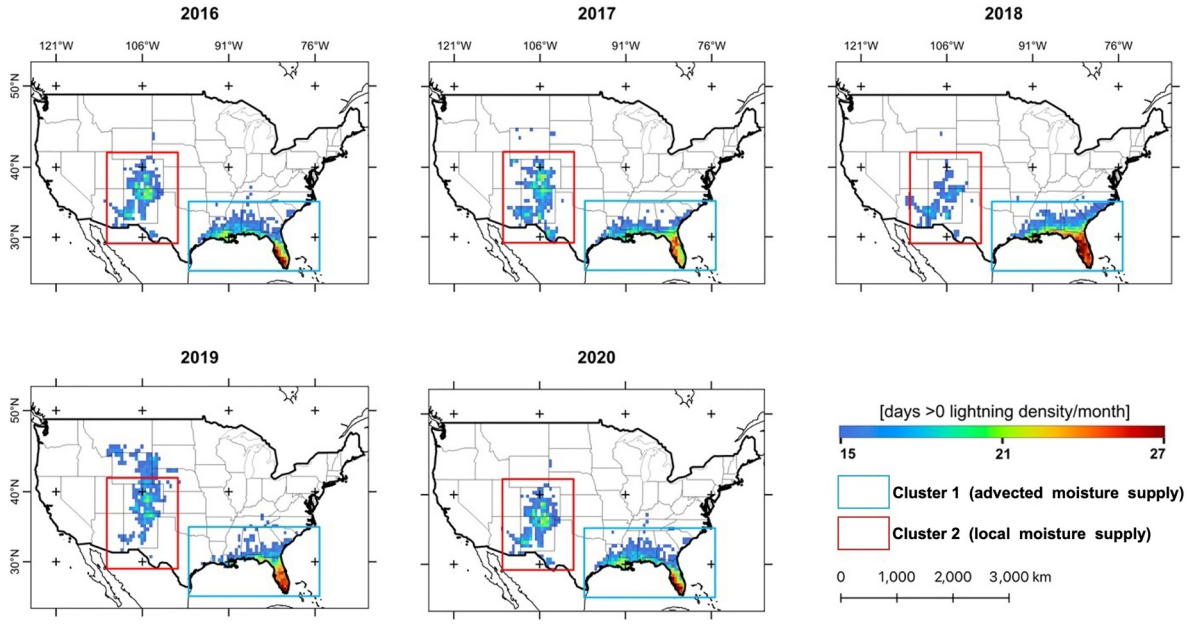

Figure 4. 90th percentile of thunderdays (TD) in CONUS in summer (JJA) from 2016 to 2020 showing two distinct pixel clusters, each with high TD occurrence. Cluster 1—blue box, along the Gulf Coast—is persistently humid, with high SM, TWS, and CAPE year-round. Cluster 2—red box, centered on the Southern Rockies—is less humid, except when under the influence of the summertime North American Monsoon.

TWV (Chakraborty et al., 2021; Prein et al., 2017; T. Zhang et al., 2021). SM-LD$_w$ correlations are very similar to SM-LD correlations (lowered by ∼2%). Overall, summer months exhibit the highest correlations, due to higher lightning occurrence yielding higher statistical signal-to-noise ratios.

Because of the zero-inflated nature of LD and LD$_w$ correlations are highest where frequency (TD) is highest. Because of this, statistical relationships have the highest power in the Southeast region. To investigate possible land-cover factors effecting lightning, data from NLCD was used to map discrete land-cover classes. The original 16 land-cover classes were reclassified, concentrating on four primary categories: urban, agricultural land, forest, and wetlands for examination. In the Southeast, wetlands are notably widespread and are unique in their near-constant moisture supply, low continentality, and ocean-like Bowen ratios. Across space, within regions categorized as wetland, the mean moisture supply (as represented by SM) was positively correlated with lightning intensity: r(SM, LD$_w$) values range from 0.49 to 0.77 for individual years. While there are confounding geographical covariates, such as distance to ocean and associated weather systems, this is a notable outlier to the rule-of-thumb that continental convection tends to organize and intensify over the relatively drier areas near water sources rather than over the water sources themselves (Klein & Taylor, 2020; Taylor et al., 2011).

In agricultural areas, the spatial SM-LD$_w$ correlation fluctuates from $r = 0.4$ to 0.53, with an average $\bar{r} = 0.47$ from 2016 to 2020. Forested regions show the least covariation between mean soil moisture and lightning intensity with values r(SM, LD$_w$) ranging from $r = 0.18$ to 0.45 ($\bar{r} = 0.27$). This implies diverging land-atmosphere relationships for lightning storm intensity across landscapes. To fully investigate the reasons for these differences would require careful separation of mechanisms, timescales, spurious statistical artifacts, and physical feedbacks (Salvucci et al., 2002), but could shed light on the interactions between long-term convection climatology and short-term land-atmosphere feedbacks. Future work could more systematically investigate the influence of land cover type and interannual variability on SM–LD relationships by combining longer time series with physically based modeling approaches.

Outside of the Southeast region, land-cover patterns were masked by low correlation signals due to low frequency (TD). To control for the role of frequency in the analyses, we subsetted our data to select only those pixels with the highest frequency of thunderdays. Figure 4 illustrates the 90th percentile of thunderday occurrences over a 5-year period in the summer months. Notably, there are consistent spatial patterns during this period, with two main pixel clusters exhibiting high thunderday density.

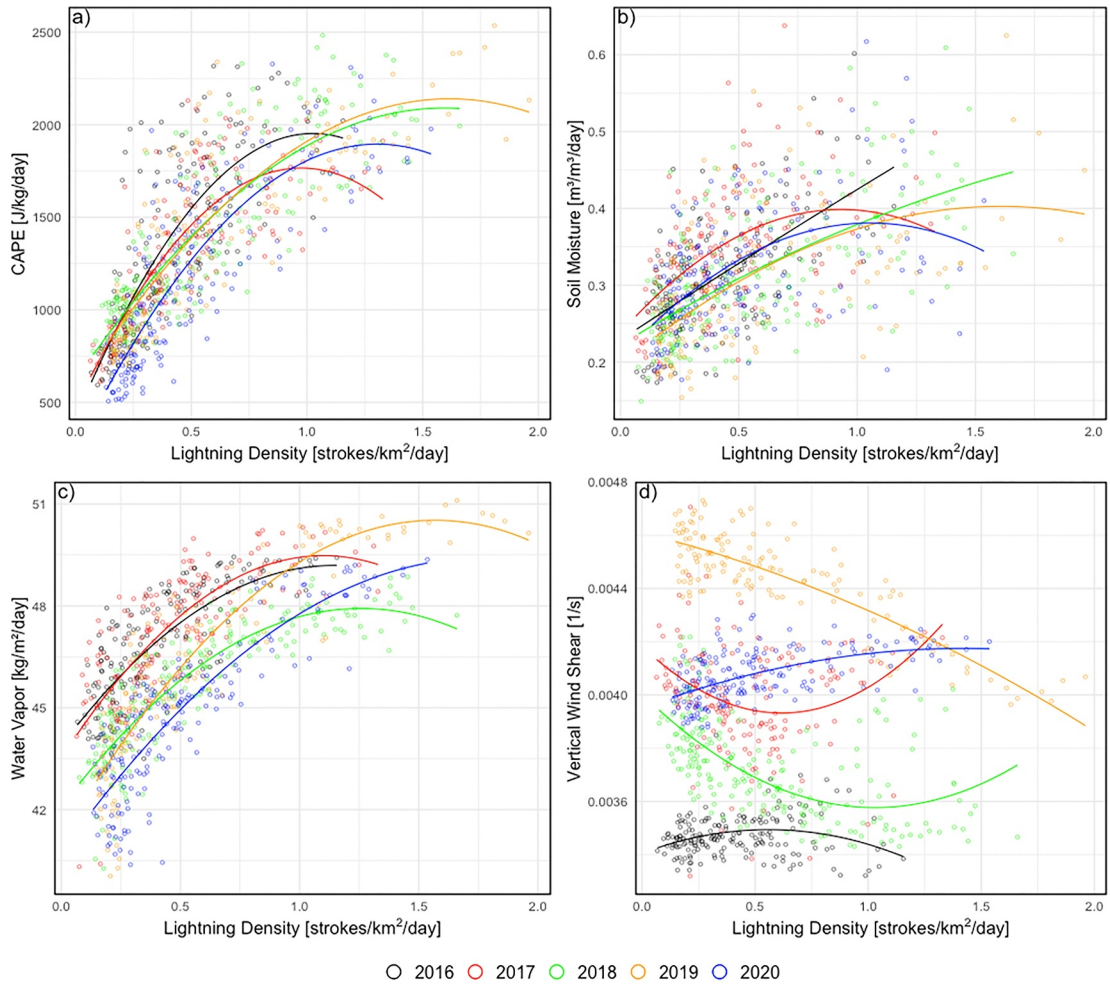

Figure 5. Cluster 1—the Gulf Coast. Cluster 1 JJA lightning density (LD) relationships with covariates, using only those locations with the highest number of thunderdays (occurrence frequency in upper decile, spatially) (a) with CAPE, (b) with SM, (c) with TWV and (d) with VWS, respectively. Each point represents one pixel's JJA value of each variable. Colors represent years. LD data points beyond three times the standard deviation are clipped for clarity. A regression function is added for better illustration of the dependence between the variables.

Cluster 1 (pixels in the blue box in Figure 4) lies along the Gulf Coast and north as far as South Carolina, primarily in the Southeast climate region (see Figure 1). Cluster 2 (pixels in the red box in Figure 4) is centered on the Southern Rockies, particularly on the New Mexico-Colorado border, encompassing most of the "Southwest" climate region (Figure 1). Rather than using the strict spatial definition, these groupings of particularly active pixels allow us to reduce statistical artifacts that can be caused by high variability in TD within a geographic region.

For pixels in Cluster 1, water supply from the surface is typically high, due to both proximity to the Gulf of Mexico and high soil water contents. The Gulf of Mexico is the dominant source of atmospheric water in the eastern CONUS, and so TWS is high here as well. While there is significant advection of water to the north across Cluster 1, the water supply is relatively local here, with CAPE typically increasing over days-to-weeks after precipitation events as the surface warms and moistens the atmosphere (L. Zhang et al., 2023). LD values are quite high, often averaging more than 1 stroke/km^2 daily throughout the summer.

All of LD, SM, TWS, and CAPE are highly correlated spatially across Cluster 1 pixels (Figure 5). Observed interannual variability in these relationships is small compared to the spatial patterns; pixels with high LD tend to also exhibit high SM, high VWC, and high CAPE. These highest LD pixels tend to be in Florida, with decreasing activity to the northwest, but the spatial pattern varies somewhat year-to-year, suggesting that some of the covariance between these variables may indeed be related to causal pathways beyond the patterns of spatial

Table 2
Pearson's Correlations (r) Between Lightning Density and Studied Variables During JJA for the Cluster 1 (CL1) and Cluster 2 (CL2) Area, Respectively

Variable	CAPE		SM		TWV		VWS	
Year	CL1	CL2	CL1	CL2	CL1	CL2	CL1	CL2
2016	0.73	0.22	0.66	0.17	0.70	0.08	0.18	−0.07
2017	0.77	0.45	0.50	0.04	0.67	0.36	−0.16	−0.28
2018	0.83	0.15	0.65	0.17	0.80	0.13	−0.54	0.05
2019	0.86	0.40	0.64	0.16	0.85	0.40	−0.80	0.52
2020	0.82	0.44	0.57	0.07	0.72	0.24	0.50	−0.06
average r ($\bar{r}$)	0.80	0.33	0.60	0.12	0.75	0.24	−0.16	0.03

climatology. Vertical wind shear shows clear interannual variability (Figure 5), but this does not appear to lead to major changes in seasonal LD. If anything, the spatial patterns suggest lower average VWS in high LD pixels. This implies that VWS is rarely the bottleneck ingredient for LD in Cluster 1, at least on seasonally-averaged scales. VWS shows a modest negative correlation with LD in the Southeast region when examined on monthly scales (Figure 3), but this relationship weakens when data are aggregated seasonally for Cluster 1 ($\bar{r} = -0.16$, Table 2). This behavior is consistent with the dominance of air-mass thunderstorms in humid, low-shear environments, where local soil moisture and boundary layer instability govern storm development (Baker et al., 2001). Seasonal averaging obscures these finer temporal variations, reducing the apparent strength of the inverse VWS-LD relationship. In contrast, Cluster 2, no meaningful correlation between VWS and LD is observed ($\bar{r} = 0.03$), likely reflecting the stronger role of monsoonal influences on convection.

For the pixels in Cluster 2, the mean across-space $\bar{r}$(LD, CAPE) from 2016 to 2021 is 0.33, whereas for Cluster 1, it is notably higher at 0.80 (Figures 5 and 6 and Table 2). A similarly strong contrast is evident for soil moisture, with Cluster 1 showing an $\bar{r}$(LD, SM) of 0.60, while Cluster 2 exhibits a much lower value of $\bar{r}$(LD, SM) = 0.12.

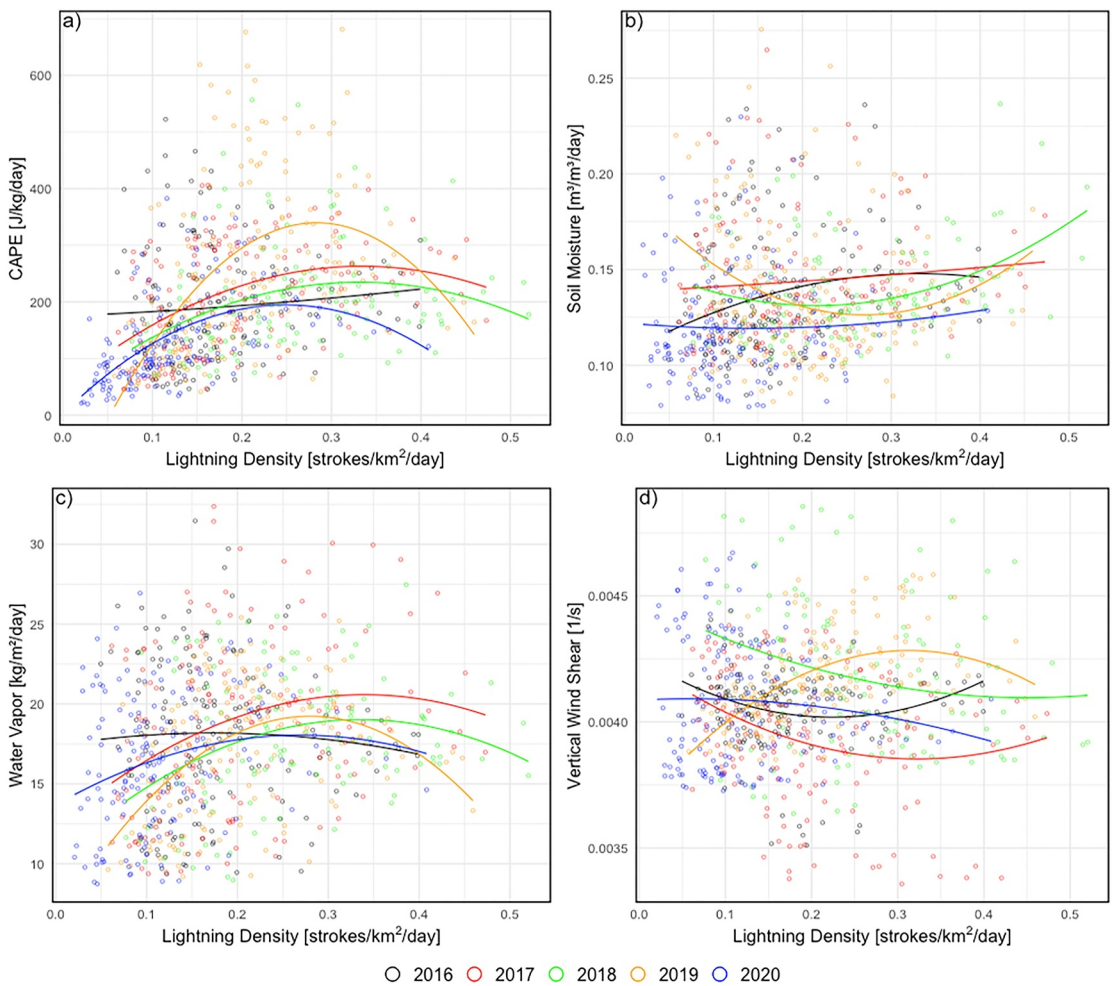

Figure 6. Cluster 2—the Southern Rockies.: Cluster 2 JJA lightning density (LD) relationships with covariates, using only those locations with the highest number of thunderdays (occurrence frequency in upper decile, spatially), as in Figure 5, (a) with CAPE, (b) with SM, (c) with TWV and (d) with VWS, respectively. Each point represents one pixel's JJA value of each variable.

Again, this likely implies that either: (a) local surface water supply rarely limits convective triggering in the wet, coastal areas of Cluster 1, but does in the more arid Cluster 2; or (b) lightning and associated precipitation are more prevalent in Cluster 1, leading to more uniformly wet soils, while Cluster 2 shows higher spatial variability in storm occurrence at monthly time-scale.

In addition to differences in soil moisture dynamics, the role of topography may also influence lightning density patterns in the southwestern United States. Cluster 2, centered at the Southern Rockies, is characterized by complex terrain. Frequent orographic lifting could act as a trigger for convection independent of surface soil moisture conditions. This terrain complexity, combined with large-scale moisture advection, may contribute to the observed weaker spatial correlations between soil moisture and lightning density in this region compared to the Southeast.

Figure 6 shows the same across-space relationships as Figure 5, but for the pixels in Cluster 2. Note that both TD and LD are generally lower in Cluster 2 by roughly a factor of two (Figures 4–6). Similarly, SM, TWV, and CAPE are typically lower in Cluster 2 by a factor of two or more.

In contrast to TD, the intensity metrics, LD_w and LD, do not show strong regional patterns. For the 90th percentile of LD_w, the peak activity was found in the Midwest, but with considerable variability, and with Florida displaying lower typical intensity values. Locations with LD above the 90th percentile spatially, are primarily in the Midwest, Upper Midwest, and Florida. The results in Figures 5 and 6 using LD_w in place of LD are similar and are shown in Appendix A (Figures A1 and A2). To further assess the robustness of the soil moisture and CAPE relationships with lightning activity, Wilcoxon rank-sum tests comparing lightning densities under high and low soil moisture and CAPE conditions across multiple years (2016–2020) for Cluster 1 and Cluster 2 were performed (Figure A3). In Cluster 1, both soil moisture and CAPE showed highly significant differences in lightning densities, with p-values consistently below 2×10^{-16}. TWV also exhibited significant relationships, though slightly weaker than CAPE but stronger than soil moisture. In contrast, in Cluster 2, the significance of soil moisture was much lower (p-values ranging from 0.008 to 0.06 across years), while CAPE remained statistically significant ($p < 0.005$).

Figure 7 shows time lags between LD and precipitation and between LD and soil moisture using a wavelet coherence analysis (WCA). The input data are at daily scale, with soil moisture snapshot retrievals at 6 a.m. local time, and daily aggregated precipitation and LD variables (midnight-to-midnight) assigned a time noon. The WCA determines the dominant temporal regressive lag of each timeseries pair within a window from 0 to 15 days in either direction for each point in time. Analyses are conducted using spatially-averaged daily values of each variable over the Florida peninsula to create a single wavelet timeseries. These time series are then smoothed using 60-day, centered, moving-window average smoother.

Throughout the results and discussion, "leading" refers strictly to temporal precedence between variables based on observational time lags and should not be interpreted as implying a causal relationship. Both lead-lag time series display a seasonal climatology, with different signs seasonally and an amplitude of one-half day, with the two time series generally out of phase. LD typically leads precipitation by a fraction of a day from June to January, and precipitation leads LD from January to June. The opposite is true for SM: SM generally leads lightning by a fraction of a day in the summer and fall, and lags in the winter and spring. This implies that a typical progression of soil moisture anomalies is associated with subsequent lightning anomalies, which in turn lead to precipitation anomalies.

4.2. Yearly Changes in Paired Soil Moisture and Lightning Density

Figure 8 depicts the variations in lightning density from year-to-year in the summer (JJA). These changes exhibit significant heterogeneity, and we explore the year-to-year variability in comparison with variables such as soil moisture (Figure 9).

Figure 8 illustrates substantial changes in lightning density (LD) throughout all studied years. Particularly notable are these fluctuations in the transitional aridity region near the 100th meridian, an area of noted hydroclimatic variability due to variable moisture convergence from the Gulf of Mexico (Koster et al., 2004; Seager et al., 2018). The region of peak variability is along the Kansas/Missouri, Oklahoma/Arkansas, and Oklahoma/Texas borders, following the Missouri and Red River Valleys. This region forms a rough dipole with the surrounding areas interannually, depending on annual patterns of moisture divergence, particularly anti-correlated with the

10.1029/2025EA004207

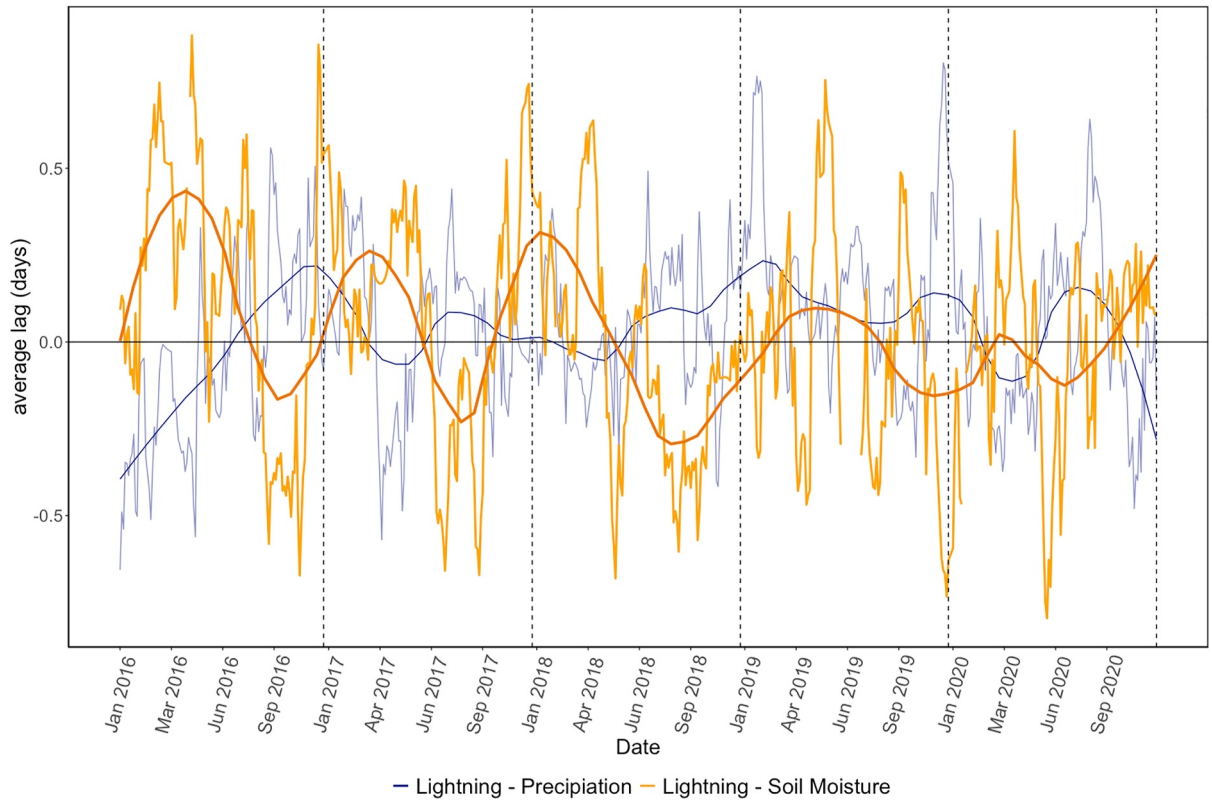

Figure 7. Time-lags of LD with precipitation and soil moisture. Average time lags for lightning versus precipitation (blue—positive denotes LD leading precipitation) and lightning versus soil moisture (orange/red—positive denotes LD leading SM) over periods ranging from 1 to 15 days.

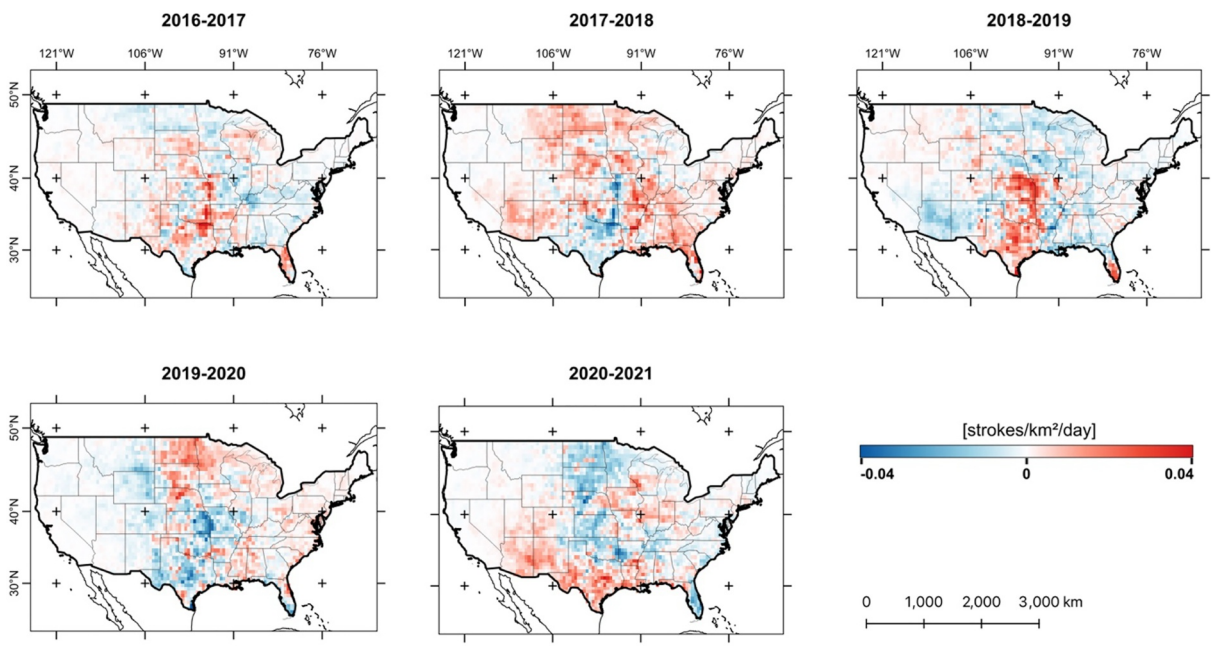

Figure 8. Year-over-year change of unweighted lightning density (LD) in CONUS during summer (JJA). Blue areas depict a decrease in strokes/km^2/day, while red areas show an increase.

10.1029/2025EA004207

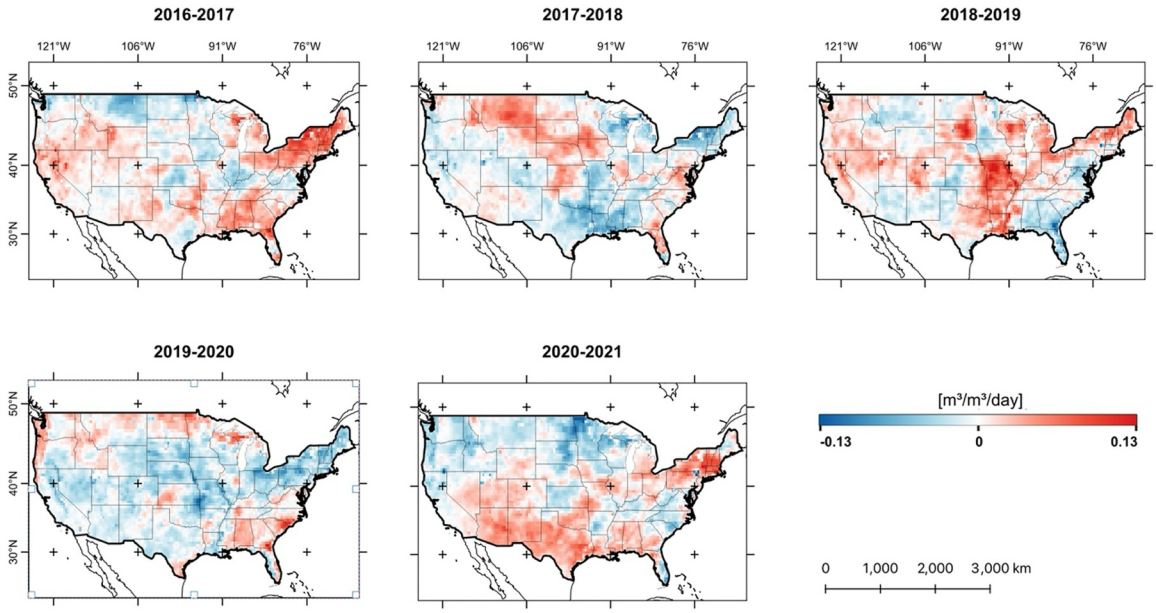

Figure 9. Year-over-year change of soil moisture in CONUS during summer (JJA). Blue areas depict a decrease in soil moisture, while red areas show an increase.

Southeast region (Figure 1). There is opportunity here for analyzing spatial patterns (e.g., empirical orthogonal functions) with decadal-scale climate indices which effect circulation in the region. West of the Rockies, interannual differences are small in absolute magnitude due to low mean LD.

Figure 9 demonstrates the variations in SM corresponding to the time periods presented in LD (Figure 8). The region of peak LD variability in Figure 8 follows the same general patterns in Figure 9, with positive correlation between SM and LD changes (more lightning co-occurring with higher SM). The same is less true in the Southeast region, which implies that the spatial patterns shown in Figure 5b (positive LD-SM correlation across pixels) may not readily translate into temporal correlations, and local SM temporal anomalies in the Southeast may not accompany similar LD anomalies.

To further investigate SM-LD co-variation, we mask interannual LD differences by conditioning on the sign of the accompanying SM changes in Figures 10 and 11.

Figure 10 shows the year-to-year changes in LD, for those pixels with a corresponding positive change in SM. Most noticeably, areas with increases in SM tended, by and large, to have increases in LD as well. By conditioning on SM increases (rather than on LD), we show wetter conditions due to all forms of precipitation—whether convective or stratiform—as well as due to higher atmospheric humidity and lower evaporative drying. Typically, locations with higher SM had higher LD, suggesting higher rates of convection.

Figure 11 shows changes in LD for the subset of pixels with negative changes in SM. Similar to Figure 10, most LD changes corresponded with the same sign changes in SM (decreases in SM most often led to decreases in LD). However, a noteworthy exception is observed in 2017–2018. During this specific timeframe, there are more pixels ($n = 1090$) indicating an increase in LD than pixels ($n = 816$) showing a decrease.

This analysis was carried out for both LD and LD_w to emphasize the differences between focusing on individual thunderstorms and overall lightning density. The non-weighted approach (LD) demonstrates a stronger correlation with soil moisture, aligning with the findings in chapter 3.1. This suggests that the year-over-year change in soil moisture appears to be more closely associated with total lightning occurrence rather than lightning intensity per storm. Upon closer inspection of histograms in Figures 10 and 11, it becomes evident that variations in soil moisture may also impact the intensity of lightning density, with a more noticeable increase in lightning density accompanying positive soil moisture changes, and vice versa.

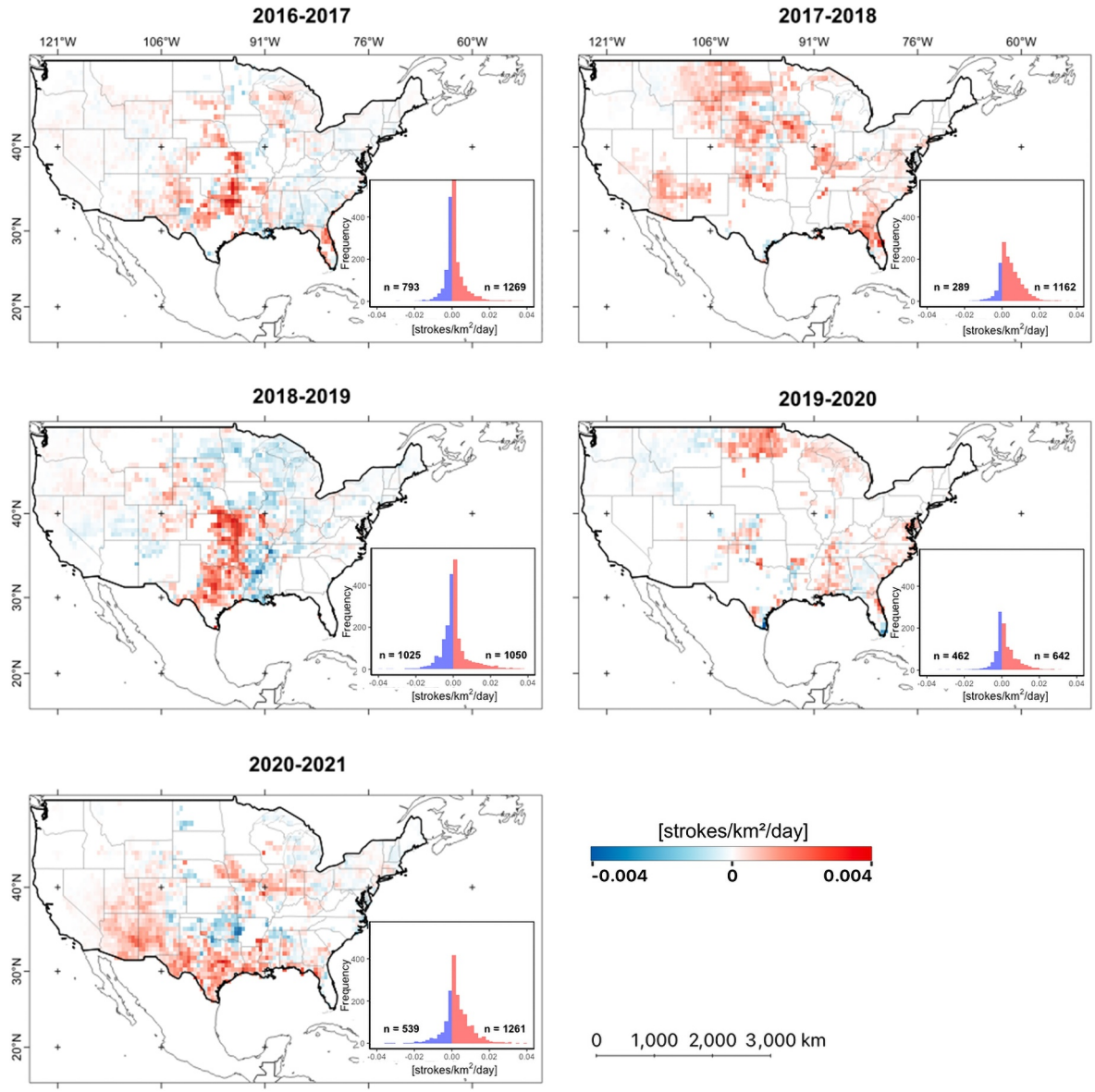

Figure 10. Year-to-year change of unweighted lightning density (LD) in CONUS (JJA) for only those pixels with accompanying positive changes in soil moisture. Blue areas depict a decrease in strokes/km^2/day, while red areas show an increase in lightning activity. The inset histograms display the distribution of change in LD for the pixels shown.

The change analysis (Δ) was applied to all remaining variables as well, though correlation mostly stayed very low when considering the entire CONUS. Across all five time periods the average correlation $\bar{r}(\Delta\text{CAPE}, \Delta\text{LD})$ is 0.37 ($\bar{r}(\Delta\text{CAPE}, \Delta\text{LD}_w) = 0.20$). For soil moisture, $\bar{r}(\Delta\text{SM}, \Delta\text{LD}) = 0.34$ ($\bar{r}(\Delta\text{SM}, \Delta\text{LD}_w) = 0.20$).

To further assess the significance of year-over-year changes in lightning density relative to soil moisture and CAPE, we performed Wilcoxon rank-sum tests across all analyzed years (2016–2020). Results indicate that soil moisture changes were significantly associated with lightning density changes in two out of 5 years (2017–2018 and 2020–2021). In contrast, CAPE changes were significantly associated with lightning density changes in 4 out of 5 years, with only 2016–2017 showing no significant group difference. Figure A4 presents boxplots summarizing these group differences, visually reinforcing the statistical results.

The correlation between soil moisture and CAPE changes is $\bar{r}(\Delta\text{CAPE}, \Delta\text{SM}) = 0.32$. The strongest across-space linear correlation in interannual differences is between total column water vapor (TWV) and CAPE, with $\bar{r}(\Delta\text{CAPE}, \Delta\text{TWV}) = 0.47$ (notably, the atmospheric humidity profile is used in the calculation of CAPE).

10.1029/2025EA004207

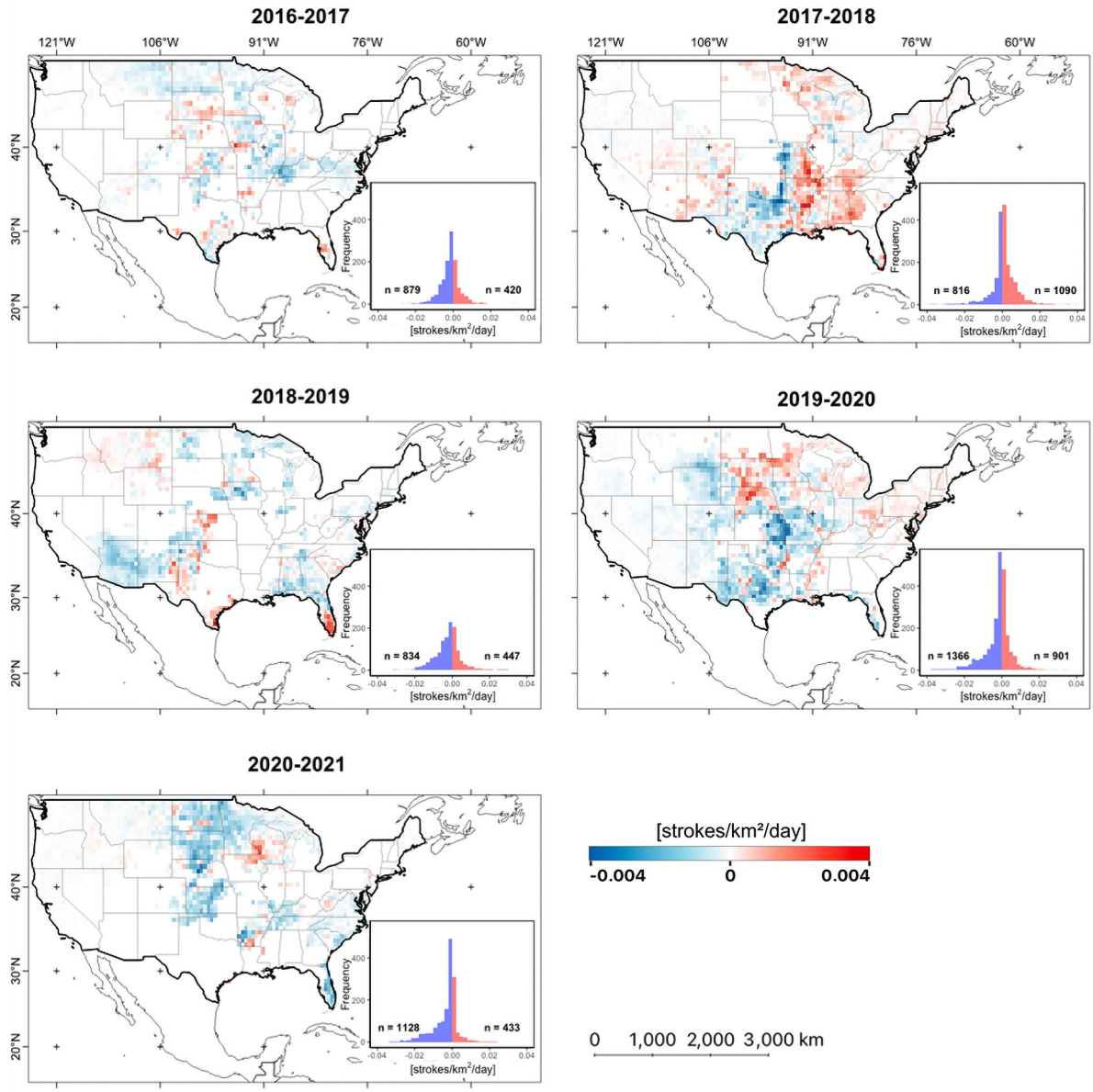

Figure 11. Year-to-year change of unweighted lightning density (LD) in CONUS (JJA) for only those pixels with accompanying negative changes in soil moisture. Blue areas depict a decrease in strokes/km^2/day, while red areas show an increase in lightning activity. The inset histograms display the distribution of change of LD for the pixels shown.

For a more detailed examination of drought patterns during these years, the SPEI product was employed. The data was downloaded in monthly intervals, aggregated into a seasonal product, and then processed into year-over-year change metric using the same methodology as applied for the other variables. The correlations between seasonal LD and the SPEI are low—$\bar{r}(\Delta\text{SPEI}, \Delta\text{LD}) = 0.19$, and $\bar{r}(\Delta\text{SPEI}, \Delta\text{LD}_w) = 0.11$, suggesting a more direct, linear relationship with soil moisture observations than an index-based proxy. A more focused examination of the "Southeast" climate region revealed similar correlations, with only minor deviations from the CONUS-wide analysis.

In a changing climate, according to Seneviratne et al. (2010) and IPCC (2021), there is a significant anticipated decrease in JJA soil moisture in the southwestern CONUS, along with a moderate decrease across much of the southern CONUS. Based on the correlational analyses, this could imply a mild decline in corresponding lightning activity across CONUS. Critically, though, these declines in SM can be caused by changes in precipitated water supply—which is a mix of stratiform and convective processes—as well as in changes in evaporative and

advective water losses from local soils. Drying caused, for example, by a so-called "accelerated hydrologic cycle" could increase CAPE generation if saturated surface parcels increase their virtual temperatures faster than the corresponding increases in environmental virtual temperatures. This could also co-occur with faster moisture recycling, increasing total column water content and the potential for convective triggering. Alternatively, if circulation changes alter the stratiform-to-convective precipitation ratio, or if convection clouds have fewer ice-ice collisions and charge transfer, LD might be expected to decrease, regardless of SM changes.

An early GCM study (Price & Rind, 1994) indicated a 30% increase in global lightning activity with warmer climatic conditions, coupled with a 24% reduction in lightning activity during cooler periods. Price (2009a, 2009b) reaffirmed this earlier work, highlighting modeled drying of specific regions due to changes in precipitation patterns and increases in evapotranspiration (ET). According to Price (2009a), this theoretically leads to fewer thunderstorms and less lightning. However, earlier models suggested an increase in thunderstorms in drier and warmer climates, proposing that storms might become less frequent but more intense, potentially resulting in a 10% increase in lightning for every degree rise due to climate change. Finney et al. (2018) criticize studies predicting increased lightning for overlooking ice flows in thunderclouds, crucial to thunderstorm formation. Their study, incorporating ice flows in a new model, suggests a 15% decrease in lightning activity by 2100 under a robust global warming scenario. These disparities underscore the immense complexity of modeling lightning under changing climate conditions.

5. Discussion

Figures 3, 5, 10, and 11 show a generally positive relationship between lightning density and soil moisture, particularly in the warm season (Figure 3). This makes sense both in terms of moisture as a crucial ingredient for CAPE and convection, and as coupled feedback from convection to precipitation to soil moisture increases. There are many ways in which this pattern can also not hold. It is common for mesoscale convective systems to be advected away from their moisture sources (Dixon et al., 2013), as well as for convective initiation to occur over dry soils upwind of moist areas (Taylor et al., 2011) or further due to gravity waves (Birch et al., 2012). Convective activity and subsequent lightning activity can be non-local with surface variables as well because of persistence in weather patterns over multiple days and atmospheric spatial autocorrelation due to large-scale synoptic patterns.

Convective feedbacks in the transitional region of peak interannual variability—near 100°W longitude—have previously been found to be driven largely by sensible heat flux (Song et al., 2016), which is a sign that soil moisture—a strong control on latent and sensible heat partitioning—can play a key role in both directions of coupling.

These findings align with the outcomes of the current study. For instance, in the southeastern United States, characterized by flat terrain and weak synoptic forcing during the summer months, the sea-breeze convergence phenomenon plays a significant role in the development of thunderstorms (Cloutier-Bisbee et al., 2019). The differential heating between the ocean and the landmass results in sea-land wind circulations, creating convergence zones on most late spring and summer days (Byers & Rodebush, 1948).

Baker et al. (2001) conducted a study involving idealized numerical simulations of convection in Florida to comprehend the roles of various factors in sea-breeze-initiated precipitation. In their analysis of complex variables, soil moisture featured prominently. They found that in regions of sea-breeze convergence, the initial soil moisture content significantly influenced the timing and location of subsequent precipitation and thunderstorms. Wet soil acted as a moisture source, enhancing convective available potential energy (CAPE), and concentrating strong precipitation in already moist areas (Baker et al., 2001).

While moisture advection from oceans does contribute to moisture distribution, the impact of soil moisture in Florida during the summer months is predominantly localized, as highlighted in studies by Baker et al. (2001) and Koukoula et al. (2021). These research findings are consistent with the outcomes of the present study, which focuses on lightning dynamics.

Conducted wavelet coherence analysis (WCA) for defining variations between LD and precipitation and LD and soil moisture time series at different length scales (Figure 7) displayed a seasonal climatology, with average time lags varying between ±0.5 days. This implies that anomalies in soil moisture are associated with subsequent anomalies in LD, leading in turn to anomalies in precipitation. While this does not on its own imply a causal

relationship, it does suggest some mechanisms at play beyond the first-order storms-leading-soil moisture patterns, and supports previous evidence of soil moisture-to-precipitation feedbacks (Koukoula et al., 2021; Taylor et al., 2011; Tuttle & Salvucci, 2017). The employed WCA uses the Morlet wavelet which is "naturally robust against shifting a feature in space" (Si, 2008), meaning the method considers the phase information when calculating the coherency between two time series at different length scales and is hence, more robust compared to other wavelets, such as the Mexican hat or Harr (Si, 2008). Although, the time series that are input to the WCA are considered as nonstationary, consisting of several frequency regime (Si, 2008), autocorrelation in all of these time series at daily scale complicate the mechanistic analysis, but these could perhaps be dealt with in future studies through use of causal analyses or typical time-series analysis tools (Salvucci et al., 2002; Tuttle & Salvucci, 2017).

Cluster 2 encompassing New Mexico, Arizona, and Colorado, the synoptic and lifting forces exhibit distinct characteristics. Thunderstorm development in this region is primarily influenced by terrain-related factors, where upslope winds along the eastern Rocky Mountains often trigger afternoon thunderstorms. During the summer months, the prevailing synoptic pattern is shaped by the "North American monsoon" or "southwest monsoon," significantly affecting precipitation patterns in northwestern Mexico, New Mexico, Arizona, and Colorado. The strength of the monsoon can determine its northward extension (Becker, 2021, Figure 4 in 2019). Earlier results revealed significant discrepancies between the "South" and "Southeast" climate regions, despite both being characterized by extensive wetlands. This disparity is likely attributed to the same advective processes, wherein storms utilize a greater proportion of local moisture sources in the "Southeast" compared to the "South."

Commencing in early June, a noticeable shift occurs as the subtropical high-pressure system moves northward and intensifies due to rising summer temperatures in the southwestern United States. This high-pressure system, extending from the surface to the upper atmosphere, undergoes strengthening. As it intensifies, there is a distinct alteration in wind patterns, with winds shifting toward a more southerly direction, contrary to the typical dry westerly winds. This change in wind direction plays a crucial role in transporting moisture from the Gulf of California and, to some extent, from the Gulf of Mexico. By early September, the monsoon typically weakens, and the wind patterns revert to their original state (Becker, 2021).

Vertical wind shear, despite its recognized role in enhancing storm longevity, does not show significant correlations with lightning density. Its limited impact on pixel-level spatial correlation suggests that it does not notably influence lightning density, providing an advantage by avoiding the introduction of bias related to soil moisture analysis.

In Florida, storms are predominantly influenced by the local environment and are characterized as "air-mass" storms. In contrast, storms in the southwest and Midwest of the United States exhibit a more organized nature.

Topography likely contributes to the regional differences in the soil moisture–lightning coupling observed in this study. Complex terrain can introduce uncertainties in soil moisture retrievals from satellite radiometers, as shown in synthetic experiments (Flores et al., 2012), although operational products, like from the SMAP mission, apply dedicated corrections using high-resolution digital elevation models (O'Neill et al., 2021b). Physically, while soil moisture dynamics differ between hillslopes and flat terrain, the basic mechanisms linking soil moisture, surface fluxes, and atmospheric instability are expected to remain similar at satellite resolution (decakilometer) scales. However, orographic lift in mountainous regions such as the Southern Rockies can mechanically trigger convection, potentially reducing the role of surface moisture in initiating storms (Houze, 2012). This may partly explain the weaker SM–LD correlations in Cluster 2. Meanwhile, convective feedbacks onto soil moisture after thunderstorms are likely still active. When examining the 90th percentile of lightning density per day (LD_w) and lightning density (LD) in these regions, strong correlations are not observed. This lack of correlation implies that soil moisture is more tied to the frequency of days with lightning occurrences rather than influencing the lightning density per storm.

While the main analyses in this study focus on the continental United States, some caution is warranted when generalizing the findings on a global scale. Land-atmosphere coupling strength, lightning generation mechanisms, and soil moisture–convection feedbacks can vary substantially across different climatic zones, vegetation types, and topographic settings. Regions dominated by strong monsoonal circulations, dense tropical forests, or large elevation gradients may exhibit different coupling dynamics than observed here. Nevertheless, the general

framework of linking soil moisture availability, atmospheric instability, and convective activity provides a useful starting point for extending similar analyses to other regions in future research.

6. Summary and Conclusion

This study investigates the relationship between soil moisture conditions and coincident lightning density across CONUS. Few studies have directly linked soil moisture and lightning density across CONUS. The nationwide analyses across all climate regions revealed a robust association with CAPE and TWV, along with a distinct seasonal pattern that differentiated between warm and cold seasons. Significantly, within the Southeast region encompassing Florida, South Carolina, and parts of Mississippi and Louisiana, indications of a soil moisture-lightning density relationship were identified. Upon conducting a more in-depth analysis of the region using landcover data, it was observed that areas with higher soil moisture content exhibited stronger correlations with lightning density compared to regions with drier soils.

Given the tendency for frequent thunderstorm development in the Southeast region of CONUS, an examination of the 90th percentile of thunderdays was conducted to pinpoint areas with the highest thunderday counts for further investigation. This analysis identified two distinct regions, namely the Southeast and Southwest within CONUS. Despite both regions experiencing high thunderstorm occurrences, their relationship with soil moisture exhibited significant differences. The southeastern region demonstrated a clear association between thunderstorm frequency and soil moisture, whereas the southwestern U.S. exhibited no such correlation. This difference is hypothesized to result from variations in synoptic forcing strength and thunderstorm triggering mechanisms. In the Southeast, frequent air mass thunderstorms driven by sea breeze convergence rely on local moisture sources. Consequently, the convection associated with sea breeze convergence relies predominantly on moisture from local sources. In contrast, the southwestern region, influenced by the North American monsoon and stronger synoptic forcing, allows moisture advection from the Gulf of California. This introduces moisture and instability into an arid area, triggering storms near the Colorado Mountains or other orographic topography due to upslope winds. In summary, the findings suggest that in regions with frequent thunderstorms and weak synoptic forcing, the coupling with soil moisture becomes notably more influential.

The study delved into year-over-year changes of the studied variables, with a specific focus on interactions involving soil moisture. Year-over-year analysis showed that soil moisture changes were significantly associated with lightning density changes in two out of 5 years, while CAPE changes were significant in four out of 5 years. This indicates that CAPE exerts a stronger influence on interannual lightning variability than soil moisture across CONUS.

Throughout all research analyses, a distinction between correlations to weighted (LD_w) and to unweighted lightning density (LD) was evident. In all analyses, correlations were significantly diminished when using the normalized data set (ranging from −2% for SM and up to −20% for CAPE). This initial finding suggests that soil moisture is more directly tied to the frequency of thunderstorm occurrences than the lightning density per individual storm.

The study's main limitations include the exclusion of advection, an area that could prove valuable for future investigations to gain a more comprehensive understanding of variable impacts on lightning density. The northern U.S., influenced by a westerly wind pattern transporting moisture away from its source, may not exhibit correlations due to the neglect of this lateral moisture transfer process in the pixel-level spatial distributions examined in this study.

Furthermore, future research should explore the bidirectional causal pathways between thunderstorms and soil moisture in more detail. Aggregated means at coarse temporal resolutions (monthly and higher) will not fully capture the complexities of soil moisture-thunderstorm feedbacks. Additionally, the role of complex terrain in modifying soil moisture retrievals and providing orographic lifting mechanisms for convection suggests that topographic effects warrant further investigation in future studies. Finally, although all data sets were harmonized to a monthly temporal resolution for consistency, this aggregation, together with spatial resolution mismatches, may obscure shorter-timescale surface flux variability, mask event-scale processes such as individual thunderstorms, and weaken general spatial correlations. Nonetheless, the significant differences observed in two regions with similarly high thunderstorm occurrences, as well as time lags showing a clear seasonal pattern where in summer soil moisture often leads lightning, provide compelling evidence of this relationship. Moreover, the

analyses examining the year-to-year changes in soil moisture and their correlation with lightning density are constrained by the limited temporal length of available data. The study exclusively employs a single algorithm and sensor for soil moisture measurements, emphasizing a focused and consistent approach. Although the studied years reveal noteworthy trends, a 5-year timeframe does not meet the criteria for a robust climatological analysis. Therefore, the study should be re-evaluated when longer data periods become available to ensure more comprising conclusions, especially toward climatic aspects.

Finally, this research study contributes to discover and illuminate the intricate relationship between soil moisture and subsequent lightning density. These findings have the potential to enhance thunderstorm forecasting and modeling. In addition, they provide valuable insights into how these variables, connected through the terrestrial energy and water balances and land-atmosphere feedbacks, may impact lightning initiation.

Appendix A

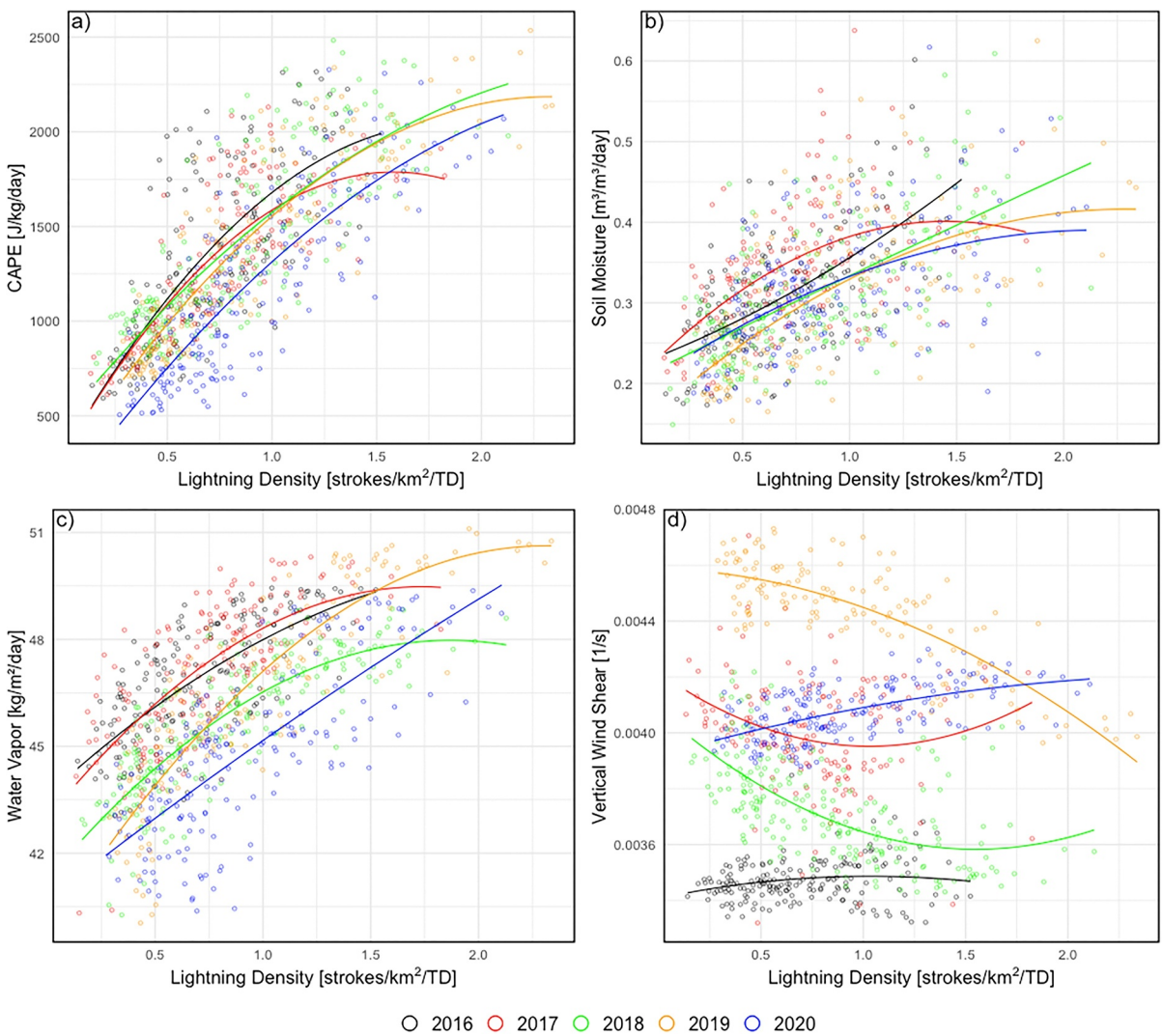

Figure A1. Lightning density (LD_w) masked by the 90th percentile of thunderdays for summer 2016–2020 (JJA) for the Cluster 1 area. (a) with CAPE, (b) with SM, (c) with TWV and (d) with VWS, respectively. Lightning data points beyond three times the standard deviation are clipped for clarity. A regression function is added for better illustration of the dependence between the variables.

10.1029/2025EA004207

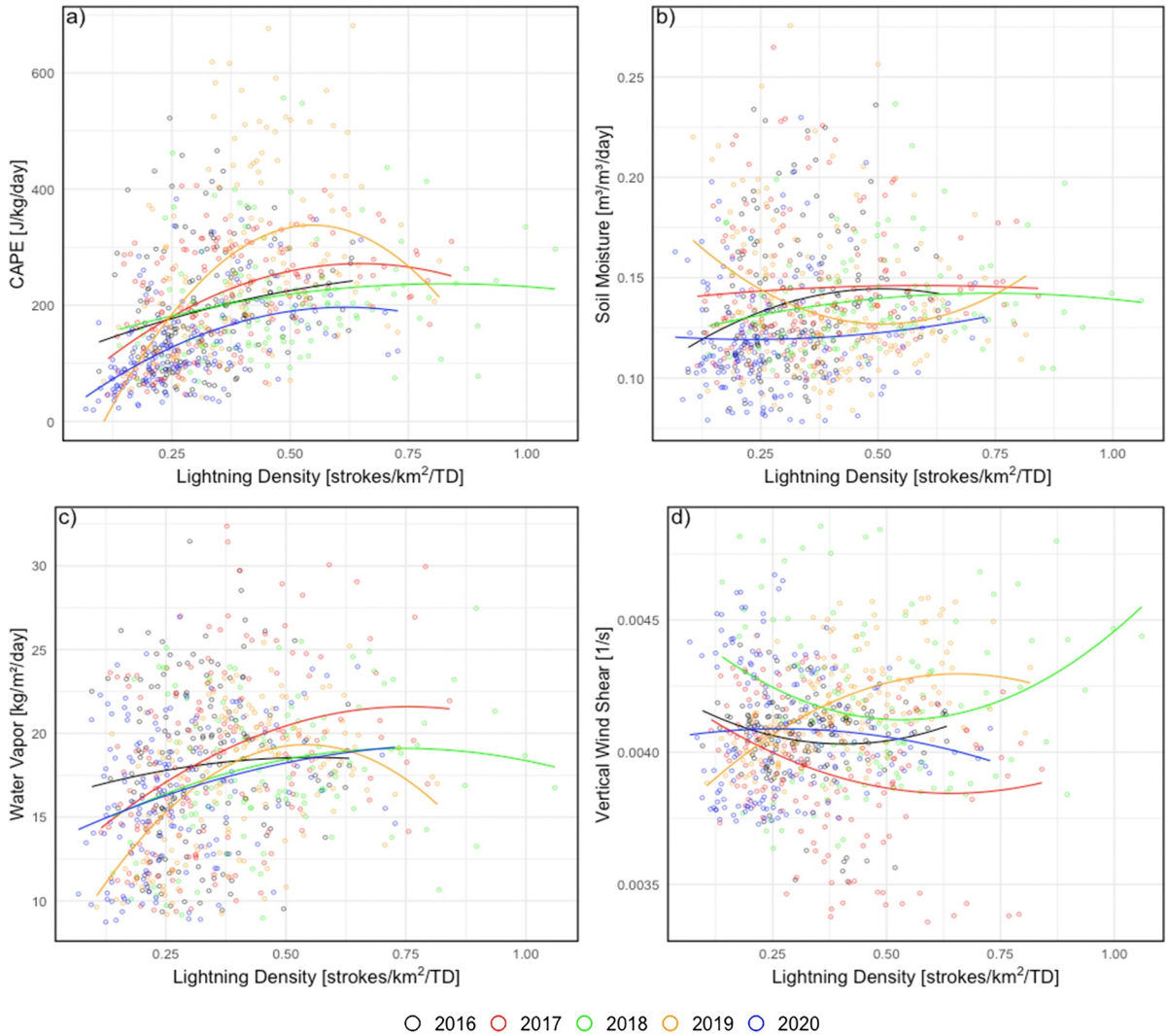

Figure A2. Lightning density (LD_w) masked by the 90th percentile of thunderdays for summer 2016–2020 (JJA) for the Cluster 2 area. (a) with CAPE, (b) with SM, (c) with TWV and (d) with VWS, respectively. Lightning data points beyond three times the standard deviation are clipped for clarity. A regression function is added for better illustration of the dependence between the variables.

10.1029/2025EA004207

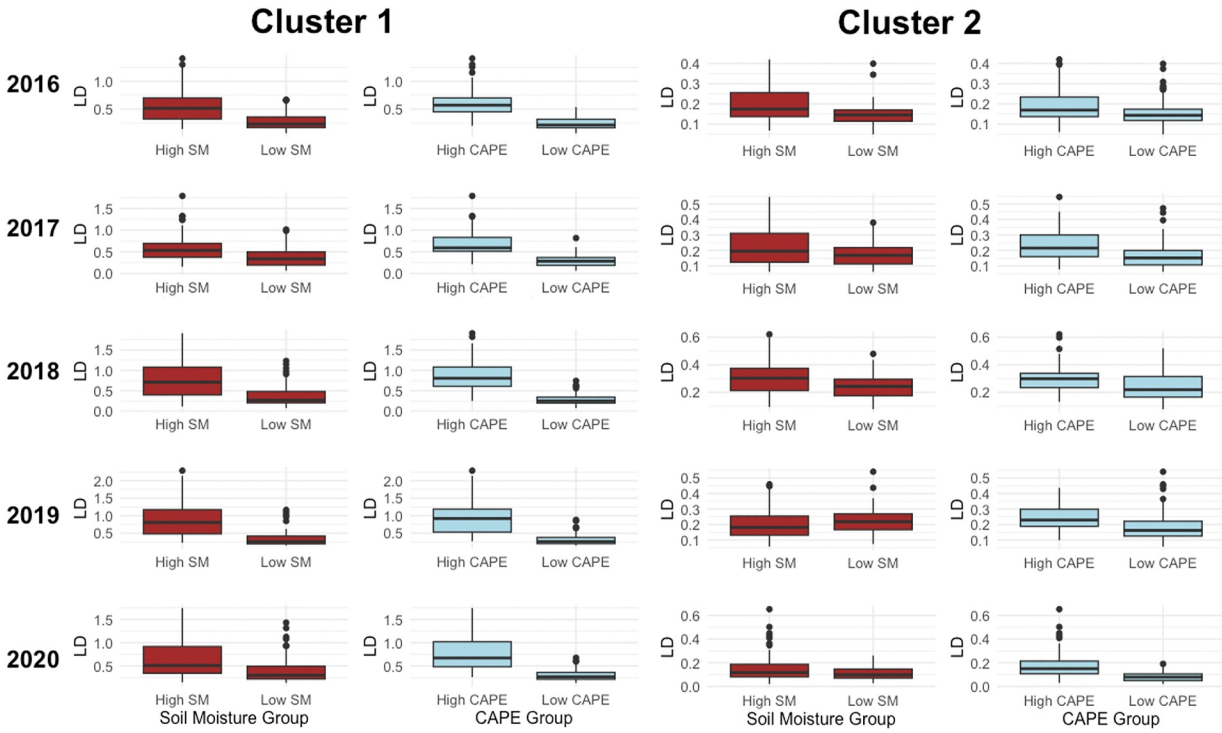

Figure A3. Boxplots showing LD for high and low SM groups and high and low CAPE groups across 2016–2020, separated by Cluster 1 (left) and Cluster 2 (right). In Cluster 1, Wilcoxon rank-sum tests revealed highly significant differences ($p < 0.001$) between high and low SM groups and between high and low CAPE groups across all years. In Cluster 2, the differences were weaker and more variable across years. For soil moisture, p-values ranged from 0.008 to 0.059, indicating some statistically significant relationships but generally less robust than in Cluster 1. CAPE differences in Cluster 2 were generally weaker, though remained largely significant ($p < 0.005$) across years.

10.1029/2025EA004207

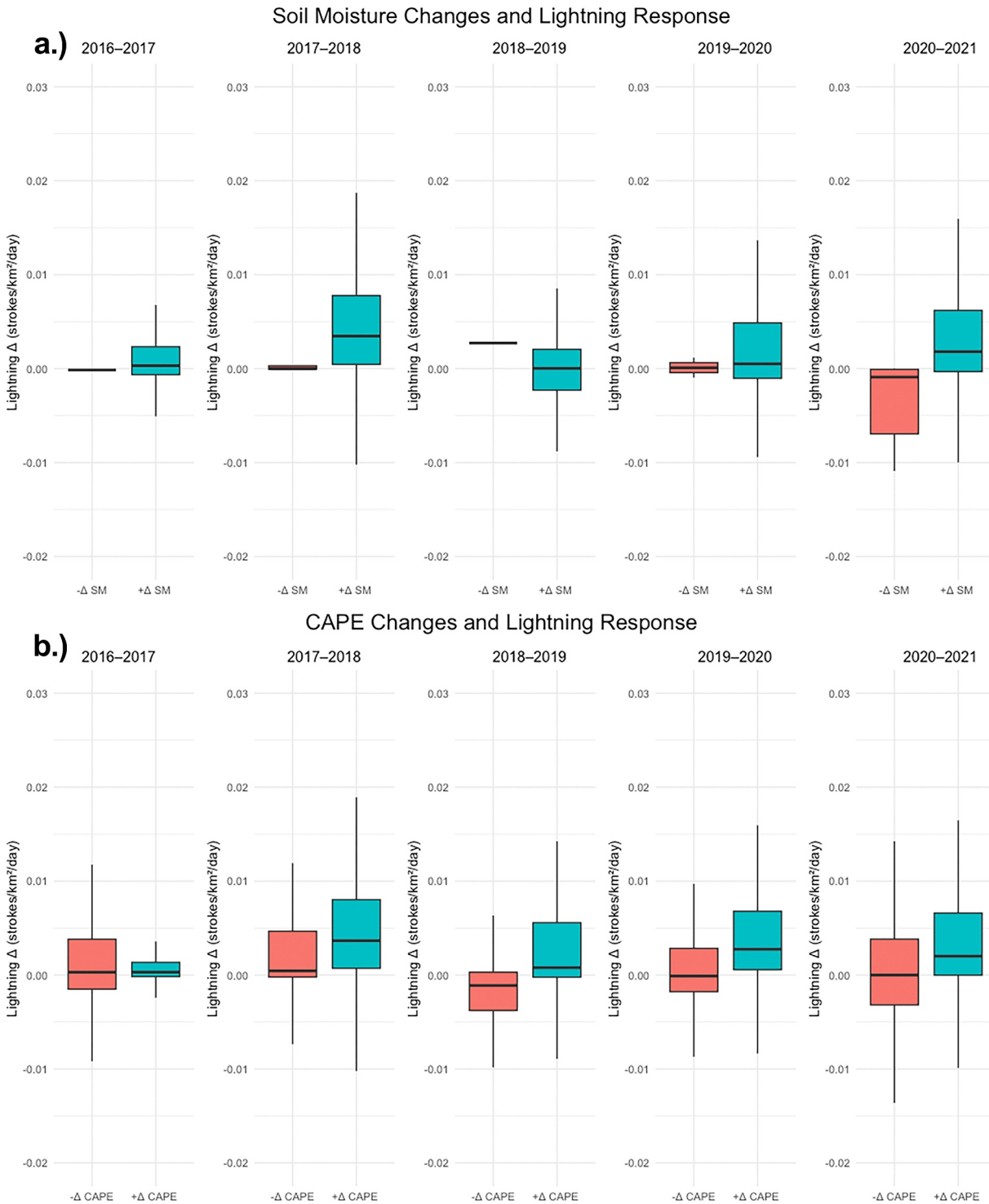

Figure A4. Boxplots showing distributions of year-over-year changes in LD grouped by positive and negative changes in (a) soil moisture and (b) CAPE across CONUS during JJA for the years 2016–2020. Statistical differences between groups were assessed using Wilcoxon rank-sum tests. Soil moisture changes were significantly associated with lightning activity in two out of 5 years (2017–2018 and 2020–2021), while CAPE changes showed significant group differences in four out of 5 years.

Table A1
List of Terminologies and Abbreviations

Abbreviation	Meaning
LD	Lightning Density
TD	Thunderdays
LD_w	Weighted Lightning Density
SM	Soil Moisture
CAPE	Convective Available Potential Energy
TWV	Total Column Water Vapor
VWS	Vertical Wind Shear
P	Precipitation
SPEI	Standardized Precipitation Evapotranspiration Index
NLCD	National Land Cover Database
ERA5	Fifth Generation ECMWF Atmospheric Reanalysis
NARR	North American Regional Reanalysis
SMAP	Soil Moisture Active Passive
WWLLN	World Wide Lightning Location Network
WGLC	WWLLN Global Lightning Climatology
CIN	Convective Inhibition
CONUS	Contiguous United States
GCOS	Global Climate Observing System
IFS	Integrated Forecast System
ET	Evapotranspiration
GCM	General Circulation Model
WCA	Wavelet Coherence Analysis
NCEP	National Centers for Environmental Prediction

Data Availability Statement

The lightning data (LD) used for analyzing global gridded lightning climatology in this study are available at the WGLC repository via https://doi.org/10.5194/essd-2021-89 under open access (Kaplan & Lau, 2021). The soil moisture data (SM) used for assessing soil moisture variability in the study are available at the NASA National Snow and Ice Data Center Distributed Active Archive Center via https://doi.org/10.5067/OMHVSRGFX38O under open access (O'Neill et al., 2021a). The reanalysis data (VWS) used for understanding wind shear patterns in this study are available at the North American Regional Reanalysis (NARR) repository via https://doi.org/10.1175/bams-87-3-343 under open access (Mesinger et al., 2006). The climate data (CAPE, TWV, P) used for evaluating atmospheric instability, precipitation and total water vapor in the study are available at the Copernicus Climate Change Service (C3S) Climate Data Store (CDS) via https://doi.org/10.24381/cds.adbb2d47 under open access (Hersbach et al., 2023). The drought indices (SPEI) used for assessing drought conditions (version SPEIbase v2.9) in the study are available at the Global SPEI Database via https://spei.csic.es/database.html under open access (SPEI, 2023). The land cover data used for analyzing surface characteristics in the study are available at the National Land Cover Database (NLCD) repository via https://doi.org/10.5066/P9KZCM54 under open access (Dewitz and USGS, 2021). Version 4.2.3 of R software used for statistical analyses and visualization in this study is preserved at https://cran.r-project.org/, available under GPL-2 license, and developed openly at the Comprehensive R Archive Network (CRAN). Version 3.32 of QGIS software used for geospatial data analysis and mapping in this study is available at https://qgis.org/en/site/, distributed under the GNU General Public License (GPL). The software is developed openly and maintained by the QGIS Project.

Acknowledgments
The authors gratefully acknowledge the use of multiple open-access data sets that enabled this research. We extend our special thanks to Kaplan and Lau for providing the global gridded lightning climatology data set. Their openly accessible lightning data were essential to this study, especially given the commercial nature of most other lightning data sources. Without their contribution, this research would not have been possible in the absence of dedicated funding. Open Access funding enabled and organized by Projekt DEAL.

References

Aich, V., Holzworth, R., Goodman, S., Kuleshov, Y., Price, C., & Williams, E. (2018). Lightning: A new essential climate variable. *Eos*, *99*. https://doi.org/10.1029/2018eo104583

Baker, R. D., Lynn, B. H., Boone, A., Tao, W.-K., & Simpson, J. (2001). The influence of soil moisture, coastline curvature, and land-breeze circulations on sea-breeze-initiated precipitation. *Journal of Hydrometeorology*, *2*(2), 193–211. https://doi.org/10.1175/1525-7541(2001)002%3C0193:tiosmc%3E2.0.co;2

Becker, E. (2021). The North American monsoon [online] Retrieved from https://www.climate.gov/news-features/blogs/enso/north-american-monsoon

Betts, A. K. (2009). Land-surface-atmosphere coupling in observations and models. *Journal of Advances in Modeling Earth Systems*, *1*(3), 4. https://doi.org/10.3894/JAMES.2009.1.4

Birch, C. E., Parker, D. J., O'Leary, A., Marsham, J. H., Taylor, C. M., Harris, P. P., & Lister, G. M. S. (2012). Impact of soil moisture and convectively generated waves on the initiation of a West African mesoscale convective system. *Quarterly Journal of the Royal Meteorological Society*, *139*, 1712–1730. https://doi.org/10.1002/qj.2062

Brisson, E., Blahak, U., Lucas-Picher, P., Purr, C., & Ahrens, B. (2021). Contrasting lightning projection using the lightning potential index adapted in a convection-permitting regional climate model. *Climate Dynamics*, *57*(7–8), 2037–2051. https://doi.org/10.1007/s00382-021-05791-z

Byers, H. R., & Rodebush, H. R. (1948). Causes of thunderstorms of the Florida Peninsula. *Journal of the Atmospheric Sciences*, *5*(6), 275–280. [online]. https://doi.org/10.1175/1520-0469(1948)005%3C0275:COTOTF%3E2.0.CO;2

Chakraborty, R., Chakraborty, A., Basha, G., & Ratnam, M. V. (2021). Lightning occurrences and intensity over the Indian region: Long-term trends and future projections. *Atmospheric Chemistry and Physics*, *21*(14), 11161–11177. https://doi.org/10.5194/acp-21-11161-2021

Chen, J., Dai, A., Zhang, Y., & Rasmussen, K. L. (2020). Changes in convective available potential energy and convective inhibition under global warming. *Journal of Climate*, *33*(6), 2025–2050. https://doi.org/10.1175/jcli-d-19-0461.1

Cloutier-Bisbee, S. R., Raghavendra, A., & Milrad, S. M. (2019). Heat waves in Florida: Climatology, trends, and related precipitation events. *Journal of Applied Meteorology and Climatology*, *58*(3), 447–466. [online]. https://doi.org/10.1175/JAMC-D-18-0165.1

Dewan, A., Ongee, E. T., Rafiuddin, M., Rahman, M. M., & Mahmood, R. (2017). Lightning activity associated with precipitation and CAPE over Bangladesh. *International Journal of Climatology*, *38*(4), 1649–1660. https://doi.org/10.1002/joc.5286

Dewitz, J., & U.S. Geological Survey (USGS). (2021). National land cover database (NLCD) 2019 products (ver. 2.0, June 2021) [Dataset]. *U.S. Geological Survey data release*. https://doi.org/10.5066/P9KZCM54

Dixon, N. S., Parker, D. J., Taylor, C. M., Garcia-Carreras, L., Harris, P. P., Marsham, J. H., et al. (2013). The effect of background wind on mesoscale circulations above variable soil moisture in the Sahel. *Quarterly Journal of the Royal Meteorological Society*, *139*(673), 1009–1024. https://doi.org/10.1002/qj.2012

Doswell, C. A., Brooks, H. E., & Maddox, R. A. (1996). Flash flood forecasting: An ingredients-based methodology. *Weather and Forecasting*, *11*(4), 560–581. https://doi.org/10.1175/1520-0434(1996)011%3C0560:fffaib%3E2.0.co;2

Emanuel, K. (2023). On the physics of high CAPE. *Journal of the Atmospheric Sciences*, *80*(11), 2669–2683. https://doi.org/10.1175/JAS-D-23-0060.1

Entekhabi, D., Yueh, S., O'Neill, P. E., Kellogg, K. H., Allen, A., Rajat, B., et al. (2014). SMAP handbook–soil moisture active passive: Mapping soil moisture and freeze/thaw from space.

Feldman, A. F., Short Gianotti, D. J., Dong, J., Akbar, R., Crow, W. T., McColl, K. A., et al. (2023). Remotely sensed soil moisture can capture dynamics relevant to plant water uptake. *Water Resources Research*, *59*(2), e2022WR033814. https://doi.org/10.1029/2022WR033814

Finney, D. L., Doherty, R. M., Wild, O., Stevenson, D. S., MacKenzie, I. A., & Blyth, A. M. (2018). A projected decrease in lightning under climate change. *Nature Climate Change*, *8*(3), 210–213. https://doi.org/10.1038/s41558-018-0072-6

Flores, A. N., Bras, R. L., & Entekhabi, D. (2012). Hydrologic data assimilation with a hillslope-scale-resolving model and L band radar observations: Synthetic experiments with the ensemble Kalman filter. *Water Resources Research*, *48*(8), W08509. https://doi.org/10.1029/2011WR011500

GCOS. (2023). Lightning. [online] Retrieved from https://gcos.wmo.int/en/essential-climate-variables/lightning

Guo, Z., Dirmeyer, P. A., Koster, R. D., Sud, Y. C., Bonan, G., Oleson, K. W., et al. (2006). GLACE: The global land–atmosphere coupling experiment. Part II: Analysis. *Journal of Hydrometeorology*, *7*(4), 611–625. https://doi.org/10.1175/JHM511.1

Hersbach, H., Bell, B., Berrisford, P., Biavati, G., Horányi, A., Muñoz Sabater, J., et al. (2023). ERA5 hourly data on single levels from 1940 to present [Dataset]. *Copernicus Climate Change Service (C3S) Climate Data Store (CDS)*. https://doi.org/10.24381/cds.adbb2d47

Hersbach, H., Bell, B., Berrisford, P., Hirahara, S., Horányi, A., Muñoz-Sabater, J., et al. (2020). The ERA5 global reanalysis. *Quarterly Journal of the Royal Meteorological Society*, *146*(730), 1999–2049. https://doi.org/10.1002/qj.3803

Houze, R. A., Jr. (2012). Orographic effects on precipitating clouds. *Reviews of Geophysics*, *50*(1), RG1001. https://doi.org/10.1029/2011RG000365

IPCC. (2021). Summary for policymakers. In V. Masson-Delmotte, P. Zhai, A. Pirani, S. L.Connors, C. Péan, S. Berger, et al. (Eds.), *Climate Change 2021: The Physical Science Basis. Contribution of Working Group I to the Sixth Assessment Report of the Intergovernmental Panel on Climate Change*. In Press.

Kaltenböck, R., Diendorfer, G., & Dotzek, N. (2009). Evaluation of thunderstorm indices from ECMWF analyses, lightning data and severe storm reports. *Atmospheric Research*, *93*(1–3), 381–396. https://doi.org/10.1016/j.atmosres.2008.11.005

Kang, D., Heath, N., Gilliam, R. C., Spero, T. L., & Pleim, J. (2022). Lightning assimilation in the WRF model (Version 4.1.1): Technique updates and assessment of the applications from regional to hemispheric scales. *Geoscientific Model Development*, *15*(22), 8561–8579. https://doi.org/10.5194/gmd-15-8561-2022

Kaplan, J. O., & Lau, K. H.-K. (2021). The WGLC global gridded lightning climatology and timeseries [Dataset]. https://doi.org/10.5194/essd-2021-89

Klein, C., & Taylor, C. M. (2020). Dry soils can intensify mesoscale convective systems. *Proceedings of the National Academy of Sciences of the United States of America*, *117*(35), 21132–21137. https://doi.org/10.1073/pnas.2007998117

Koss, W. J., & Karl, T. (1984). Regional and national monthly, seasonal, and annual temperature weighted by area, 1895-1983. [online] repository.library.noaa.gov. Retrieved from https://repository.library.noaa.gov/view/noaa/10238#tabs-2

Koster, R. D., Dirmeyer, P. A., Guo, Z., Bonan, G., Chan, E., Cox, P., et al. (2004). Regions of strong coupling between soil moisture and precipitation. *Science*, *305*(5687), 1138–1140. https://doi.org/10.1126/science.1100217

Koukoula, M., Schwartz, C. S., Nikolopoulos, E. I., & Anagnostou, E. N. (2021). Understanding the impact of soil moisture on precipitation under different climate and meteorological conditions: A numerical sensitivity study over the CONUS. *Journal of Geophysical Research: Atmospheres*, *126*(23). https://doi.org/10.1029/2021jd035096

Kunkel, K. E., Karl, T. R., Squires, M. F., Yin, X., Stegall, S. T., & Easterling, D. R. (2020). Precipitation extremes: Trends and relationships with average precipitation and precipitable water in the contiguous United States. *Journal of Applied Meteorology and Climatology*, *59*(1), 125–142. https://doi.org/10.1175/jamc-d-19-0185.1

Lintner, B. R., Gentine, P., Findell, K. L., D'Andrea, F., Sobel, A. H., & Salvucci, G. D. (2013). An idealized prototype for large-scale land–atmosphere coupling. *Journal of Climate*, *26*(7), 2379–2389. https://doi.org/10.1175/JCLI-D-11-00561.1

McNulty, R. (1985). National weather digest forecasting A conceptual approach to thunderstorm forecasting. [online] Retrieved from https://citeseerx.ist.psu.edu/document?repid=rep1&type=pdf&doi=76220a557ef1a5495fda49c9b8645d57ca120355

Mesinger, F., DiMego, G., Kalnay, E., Mitchell, K., Shafran, P. C., Ebisuzaki, W., et al. (2006). North American regional reanalysis [Dataset]. *Bulletin of the American Meteorological Society*, *87*(3), 343–360. https://doi.org/10.1175/bams-87-3-343

Mezuman, K., Price, C., & Galanti, E. (2014). On the spatial and temporal distribution of global thunderstorm cells. *Environmental Research Letters*, *9*(12), 124023. https://doi.org/10.1088/1748-9326/9/12/124023

Molina, M. J., & Allen, J. T. (2020). Regionally-stratified tornadoes: Moisture source physical reasoning and climate trends. *Weather and Climate Extremes*, *28*, 100244. https://doi.org/10.1016/j.wace.2020.100244

National Oceanic and Atmospheric Administration (NOAA). (2023). Ingredients for a thunderstorm. [online] Retrieved from https://www.noaa.gov/jetstream/thunderstorms/ingredients-for-thunderstorm

O'Neill, P., Bindlish, R., Chan, S., Chaubell, J., Colliander, A., Njoku, E., & Jackson, T. (2021a). L3 radiometer global daily 36 km EASE-grid soil moisture, Version 8 [Dataset]. *Boulder, Colorado USA. NASA National Snow and Ice Data Center Distributed Active Archive Center*. https://doi.org/10.5067/OMHVSRGFX38O

O'Neill, P., Bindlish, R., Chan, S., Chaubell, J., Colliander, A., Njoku, E., & Jackson, T. (2021b). Soil moisture active passive (SMAP) algorithm theoretical basis document level 2 & 3 soil moisture (Passive) data products. [online] Retrieved from https://nsidc.org/sites/default/files/l2_sm_p_atbd_rev_g_final_oct2021_0.pdf

Prein, A., Rasmussen, R., Ikeda, K., Liu, C., Clark, M. P., & Holland, G. J. (2017). The future intensification of hourly precipitation extremes. *Nature Climate Change*, *7*(1), 48–52. https://doi.org/10.1038/nclimate3168

Price, C. (2009a). Thunderstorms, lightning and climate change. In *Lightning: principles, instruments and applications* (pp. 521–535). https://doi.org/10.1007/978-1-4020-9079-0_24

Price, C. (2009b). Will a drier climate result in more lightning? *Atmospheric Research*, *91*(2–4), 479–484. https://doi.org/10.1016/j.atmosres.2008.05.016

Price, C., & Rind, D. (1994). Possible implications of global climate change on global lightning distributions and frequencies. *Journal of Geophysical Research*, *99*(D5), 10823. https://doi.org/10.1029/94jd00019

Price, C. G. (2013). Lightning applications in weather and climate research. *Surveys in Geophysics*, *34*(6), 755–767. https://doi.org/10.1007/s10712-012-9218-7

Rahmati, M., Groh, J., Graf, A., Pütz, T., Vanderborght, J., & Vereecken, H. (2020). On the impact of increasing drought on the relationship between soil water content and evapotranspiration of a grassland. *Vadose Zone Journal*, *19*(1). https://doi.org/10.1002/vzj2.20029

Romps, D. M., Charn, A. B., Holzworth, R. H., Lawrence, W. E., Molinari, J., & Vollaro, D. (2018). CAPE times P explains lightning over land but not the land-ocean contrast. *Geophysical Research Letters*, *45*(22), 12623–12630. https://doi.org/10.1029/2018gl080267

Salvucci, G. D., Saleem, J. A., & Kaufmann, R. (2002). Investigating soil moisture feedbacks on precipitation with tests of Granger causality. *Advances in Water Resources*, *25*(8–12), 1305–1312. https://doi.org/10.1016/s0309-1708(02)00057-x

Seager, R., Lis, N., Feldman, J., Ting, M., Park Williams, A., Nakamura, J., et al. (2018). Whither the 100th Meridian? The once and future physical and human geography of America's arid–humid divide. Part I: The story so far. *Earth Interactions*, *22*(5), 1–22. https://doi.org/10.1175/EI-D-17-0011.1

Seneviratne, S. I., Corti, T., Davin, E. L., Hirschi, M., Jaeger, E. B., Lehner, I., et al. (2010). Investigating soil moisture–climate interactions in a changing climate: A review. *Earth-Science Reviews*, *99*(3–4), 125–161. https://doi.org/10.1016/j.earscirev.2010.02.004

Short Gianotti, D. J., Rigden, A. J., Salvucci, G. D., & Entekhabi, D. (2019). Satellite and station observations demonstrate water availability's effect on continental-scale evaporative and photosynthetic land surface dynamics. *Water Resources Research*, *55*(1), 540–554. https://doi.org/10.1029/2018WR023726

Si, B. C. (2008). Spatial scaling analyses of soil physical properties: A review of spectral and wavelet methods. *Vadose Zone Journal*, *7*(2), 547–562. https://doi.org/10.2136/vzj2007.0040

Song, H., Ferguson, C. R., & Roundy, J. K. (2016). Land–atmosphere coupling at the southern great plains atmospheric radiation measurement (ARM) field site and its role in anomalous afternoon peak precipitation. *Journal of Hydrometeorology*, *17*(2), 541–556. https://doi.org/10.1175/JHM-D-15-0045.1

SPEI. (2023). Global SPEI database Version SPEIbase v2.9 [Dataset]. Retrieved from https://spei.csic.es/database.html

Taylor, C., Gounou, A., Guichard, F., Harris, P. P., Ellis, R. J., Couvreux, F., & De Kauwe, M. (2011). Frequency of Sahelian storm initiation enhanced over mesoscale soil-moisture patterns. *Nature Geoscience*, *4*(7), 430–433. https://doi.org/10.1038/ngeo1173

Tippett, M. K., Lepore, C., Koshak, W. J., Chronis, T., & Vant-Hull, B. (2019). Performance of a simple reanalysis proxy for U.S. cloud-to-ground lightning. *International Journal of Climatology*, *39*(10), 3932–3946. https://doi.org/10.1002/joc.6049

Tuttle, S. E., & Salvucci, G. D. (2017). Confounding factors in determining causal soil moisture-precipitation feedback. *Water Resources Research*, *53*(7), 5531–5544. https://doi.org/10.1002/2016wr019869

Westermayer, A. T., Groenemeijer, P., Pistotnik, G., Sausen, R., & Faust, E. (2017). Identification of favorable environments for thunderstorms in reanalysis data. *Meteorologische Zeitschrift*, *26*(1), 59–70. https://doi.org/10.1127/metz/2016/0754

Williams, E. R. (2017). Meteorological aspects of thunderstorms. In *Handbook of atmospheric electrodynamics, Volume I* (pp. 27–60). CRC Press.

Zhang, J., Wang, W.-C., & Leung, L. R. (2008). Contribution of land-atmosphere coupling to summer climate variability over the contiguous United States. *Journal of Geophysical Research*, *113*(D22), D22109. https://doi.org/10.1029/2008JD010136

Zhang, L. N., Short Gianotti, D. J., & Entekhabi, D. (2023). Land surface influence on convective available potential energy (CAPE) change during interstorms. *Journal of Hydrometeorology*, *24*(8), 1365–1376. https://doi.org/10.1175/JHM-D-22-0191.1

Zhang, R., Zhang, Y., Xu, L., Zheng, D., & Yao, W. (2017). Assimilation of total lightning data using the three-dimensional variational method at convection-allowing resolution. *Journal of Meteorological Research (Print)*, *31*(4), 731–746. https://doi.org/10.1007/s13351-017-6133-3

Zhang, T., Lin, W., Vogelmann, A. M., Zhang, M., Xie, S., Qin, Y., & Golaz, J.-C. (2021). Improving convection trigger functions in deep convective parameterization schemes using machine learning. *Journal of Advances in Modeling Earth Systems*, *13*(5), e2020MS002365. https://doi.org/10.1029/2020MS002365